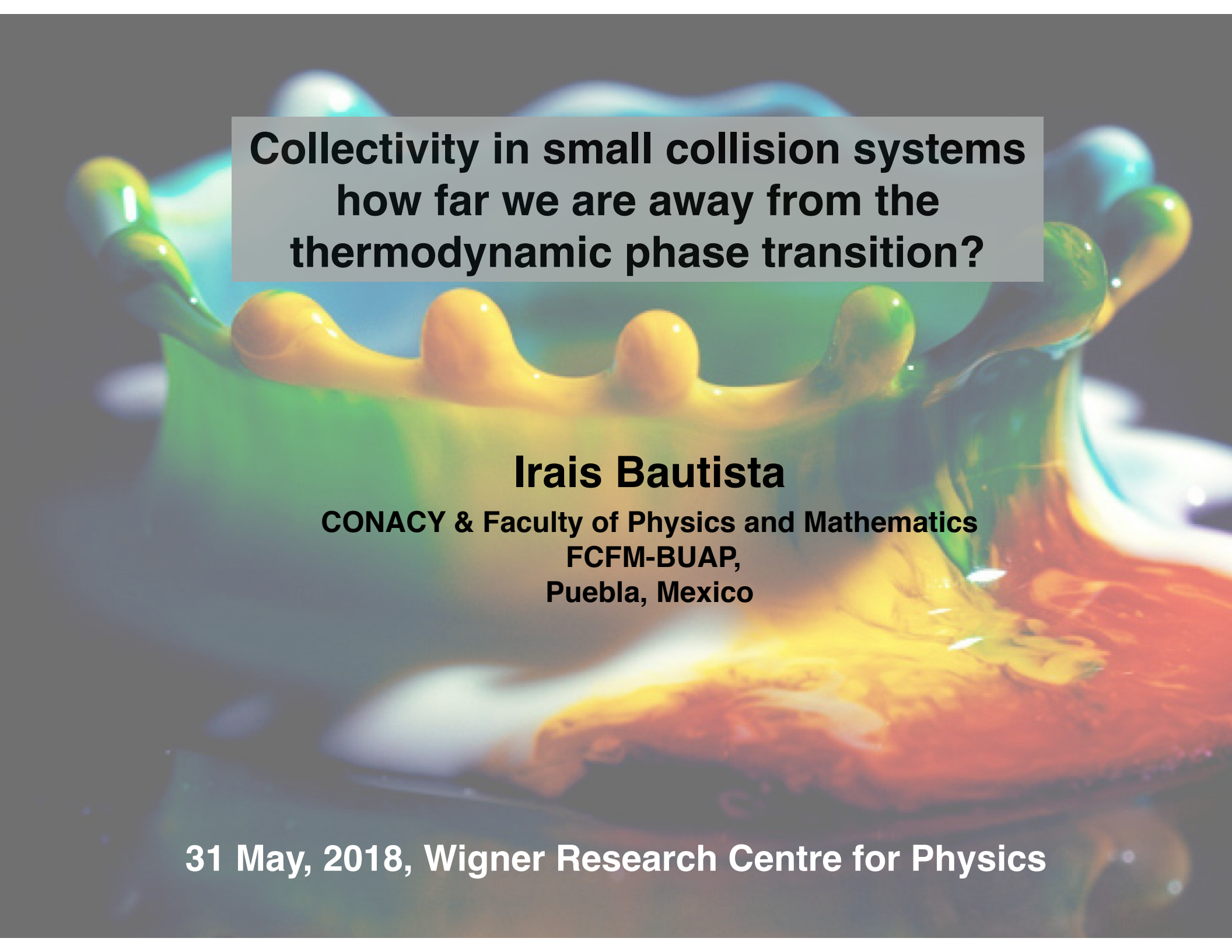

Collectivity in small collision systems how far we are away from the thermodynamic phase transition?

Irais Bautista

CONACY & Faculty of Physics and Mathematics
FCFM-BUAP,
Puebla, Mexico

31 May, 2018, Wigner Research Centre for Physics

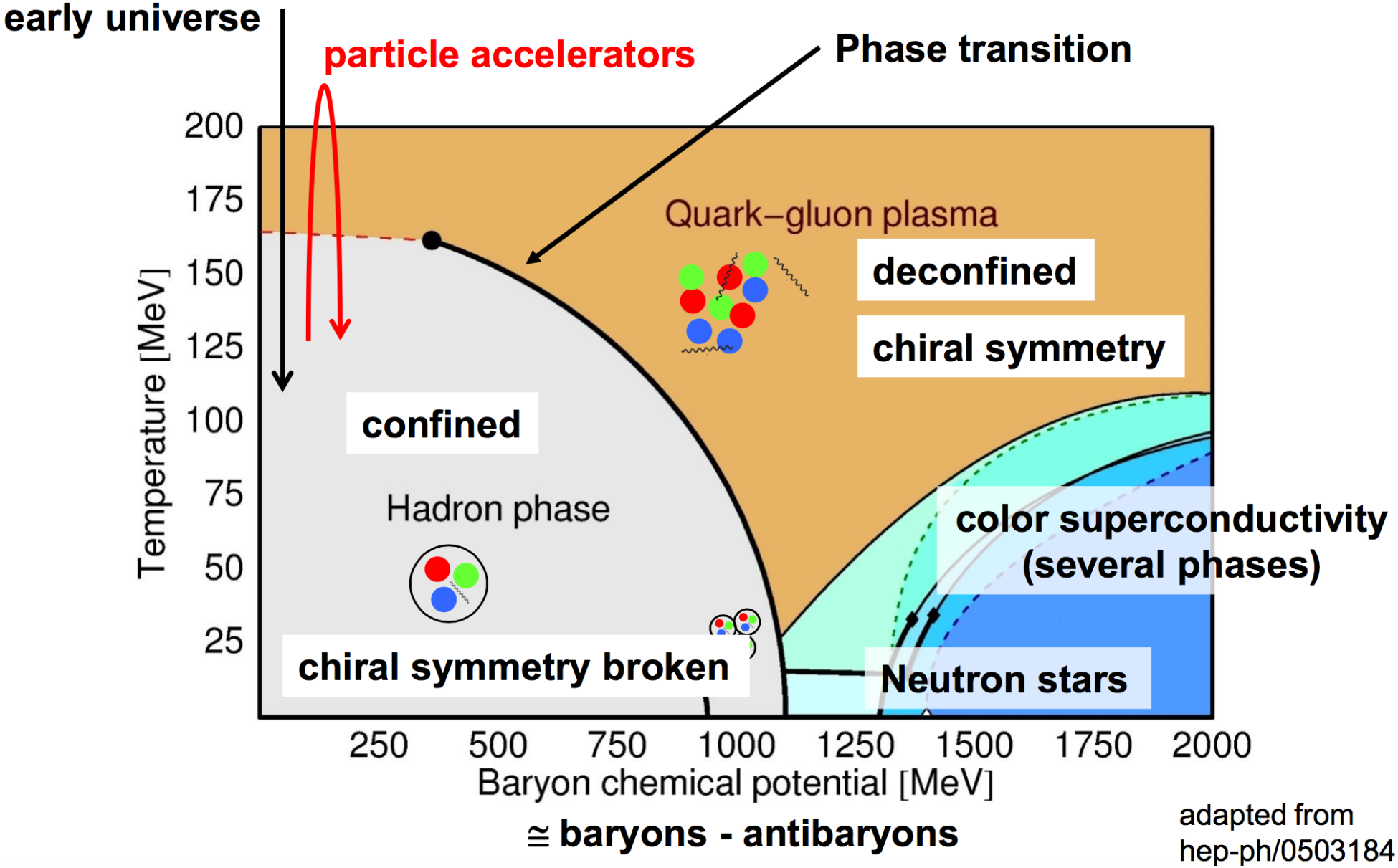
early universe
particle accelerators
Phase transition
Quark–gluon plasma
deconfined
chiral symmetry
confined
Hadron phase
color superconductivity
(several phases)
chiral symmetry broken
Neutron stars
Temperature [MeV]
200
175
150
125
100
75
50
25
250
500
750
1000
1250
1500
1750
2000
Baryon chemical potential [MeV]
≅ baryons - antibaryons
adapted from
hep-ph/0503184

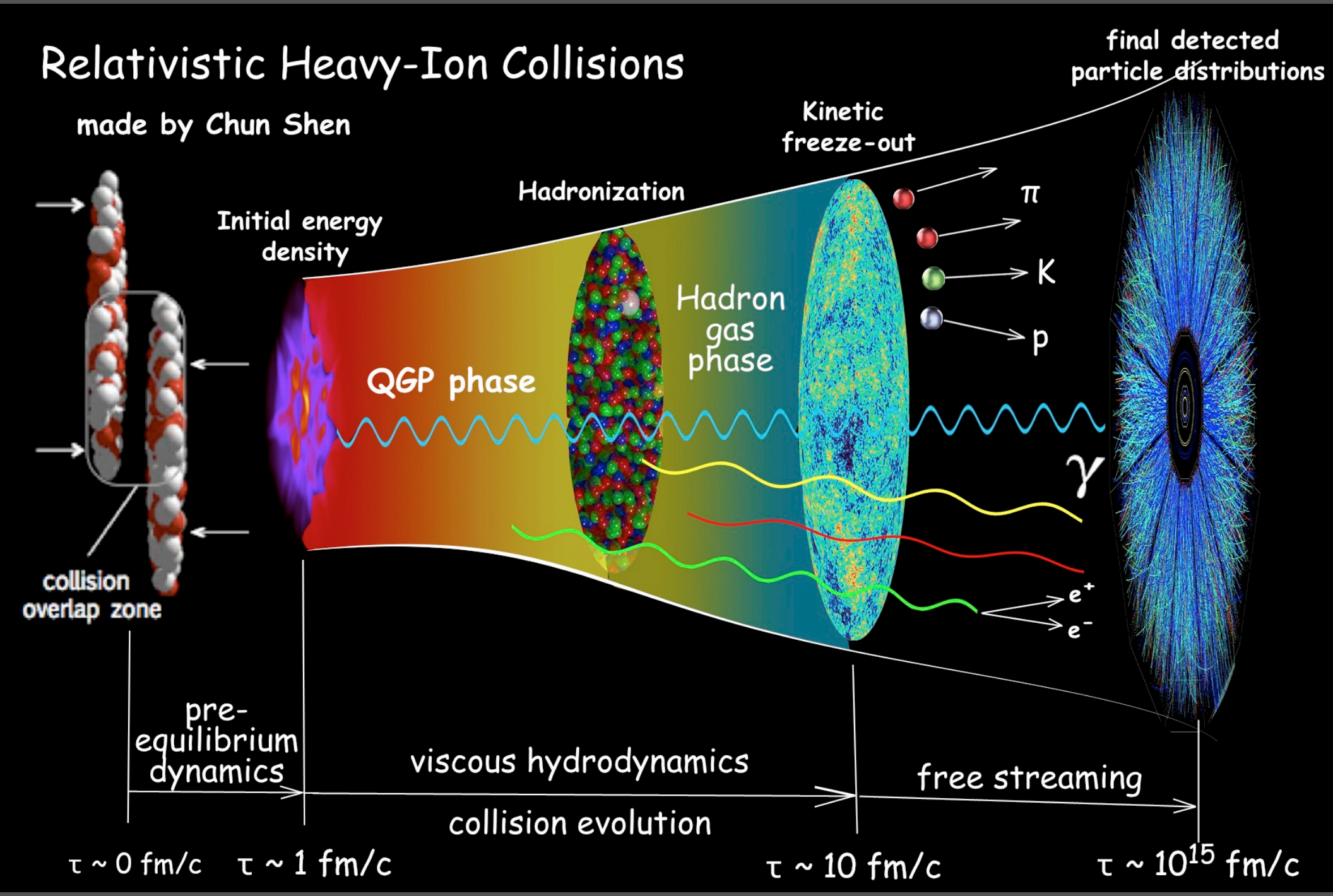
Relativistic Heavy-Ion Collisions
made by Chun Shen
final detected particle distributions
Kinetic freeze-out
Hadronization
Initial energy density
Hadron gas phase
QGP phase
π
K
p
γ
e+
e-
collision overlap zone
pre-equilibrium dynamics
viscous hydrodynamics
free streaming
collision evolution
τ ~ 0 fm/c
τ ~ 1 fm/c
τ ~ 10 fm/c
τ ~ 10^15 fm/c

Heavy Ion Collisions

4

Heavy Ion Collisions

Allows to study QCD without confinement, with quarks at their bare masses

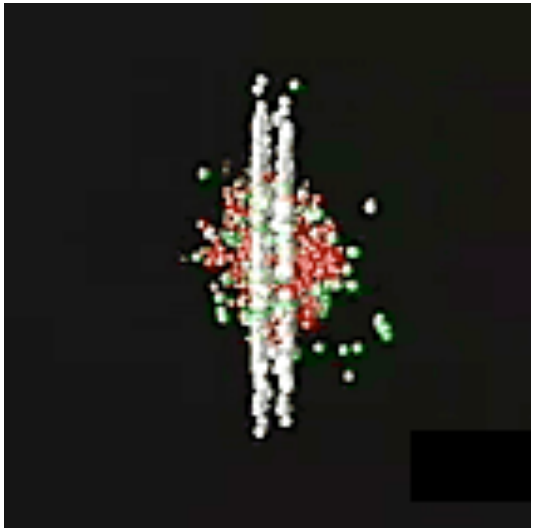

Matter at energy densities like 10 micro seconds after the Big Bang, at temperatures 105 times larger than in the sun core

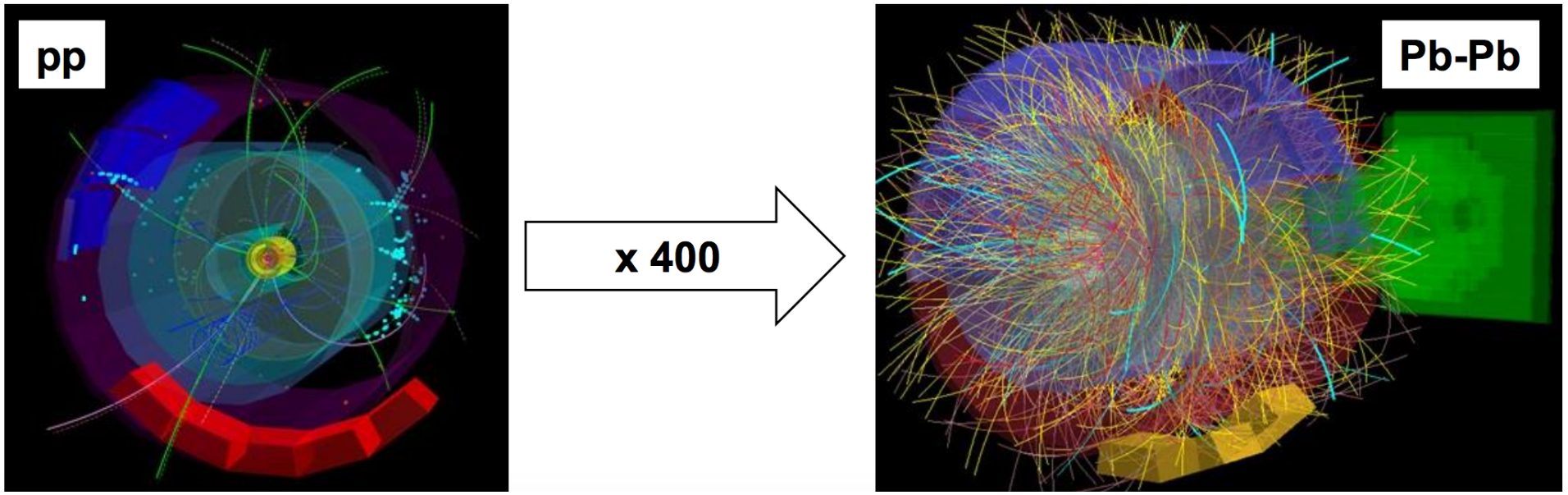

Heavy Ion Collisions

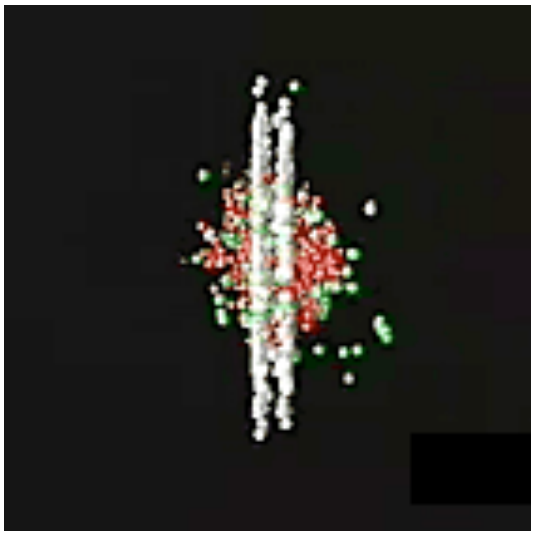

Small collision systems

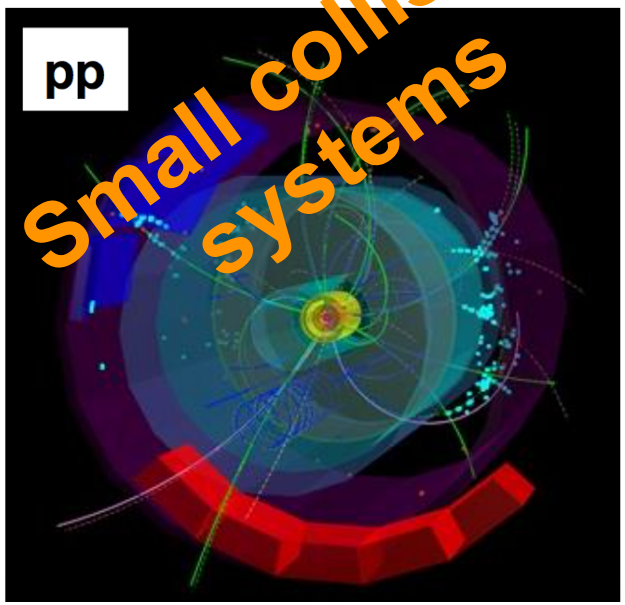

x 400

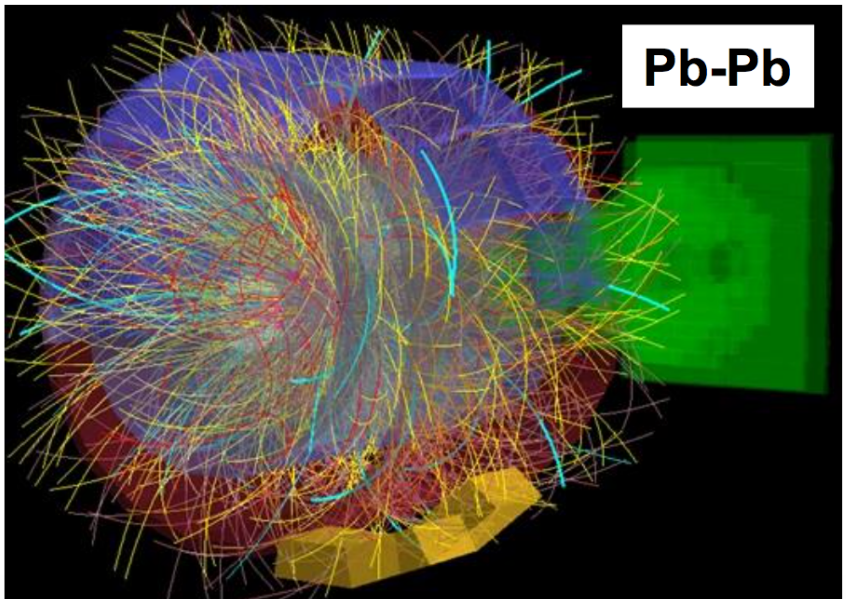

Signals of QGP

- Change on the intrinsic properties of hadrons.
- Increase the strangeness production
- Dilepton spectrum change
- J/ψ Suppression.
- Increase the production of hadron resonances
- Transverse Flow and longitudinal out of the production plane.
- Etc…

on Small systems

- In small systems, the finite-size and fluctuation effects become relevant
- Fast expansion and cooling with a lifetime of a few fm/c.

- T. S. Biro, G. G. Barnafoldi, G. Biro and K. M. Shen, J. Phys. Conf. Ser. 779 (2017) no.1, 012081
- G. Bíró, G. G. Barnaföldi, T. S. Biró and K. Ürmössy, AIP Conf. Proc 1853 (2017) 08000
- C. Gale, S. Jeon, and B. Schenke, Int. J. Mod. Phys.
- N. Armesto and E. Scomparin, Eur. Phys. J. Plus 13, 52 (2016)

Color sources

- In the transverse impact parameter plane the strings look like small disk where we can apply 2 dimensional percolation theory

$\sqrt{s}$, N_{part}

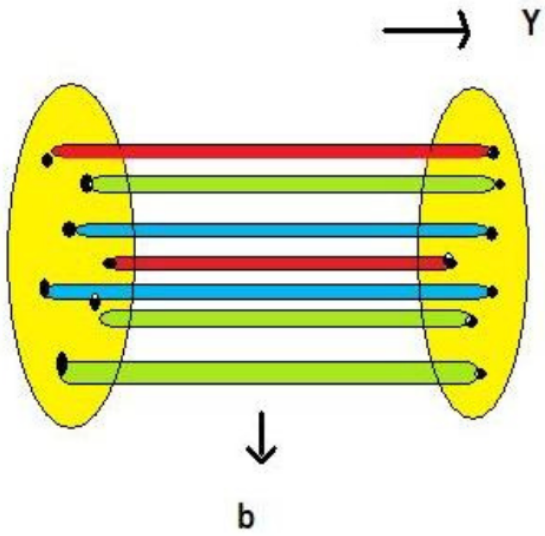

$S_1 = \pi r_0^2$

$r_0 \sim 0.25$ fm

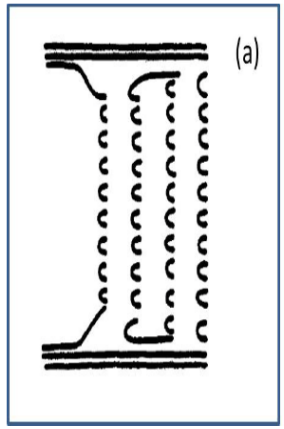

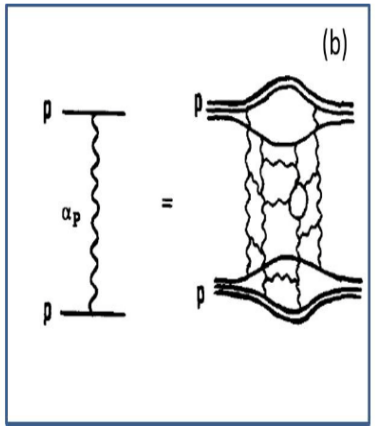

Multi particle production at high energies is currently described in terms of color strings stretched between the projectile and target.
These strings decay into new ones by production and subsequently hadronize to produce the observed hadrons.

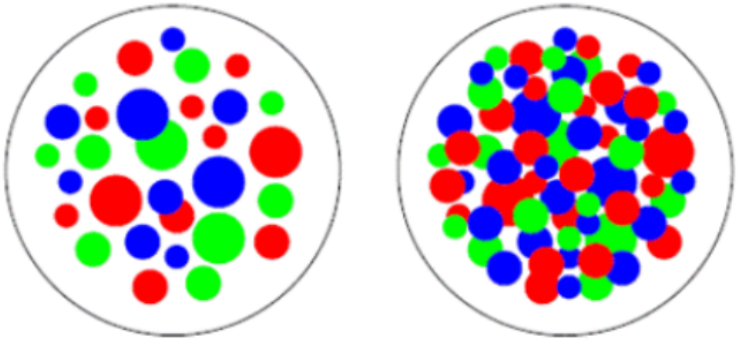

De-confinement is expected when the density of quarks and gluons becomes so high that would overlap strongly.

We have clusters within which color is not longer confined : De-confinement is thus related to cluster formation very much similar to cluster formation in percolation theory and hence a connection between percolation and de-confinement seems very likely.

String Percolation Model

- At a critical density, a macroscopic cluster appears and mark a geometric phase transition.

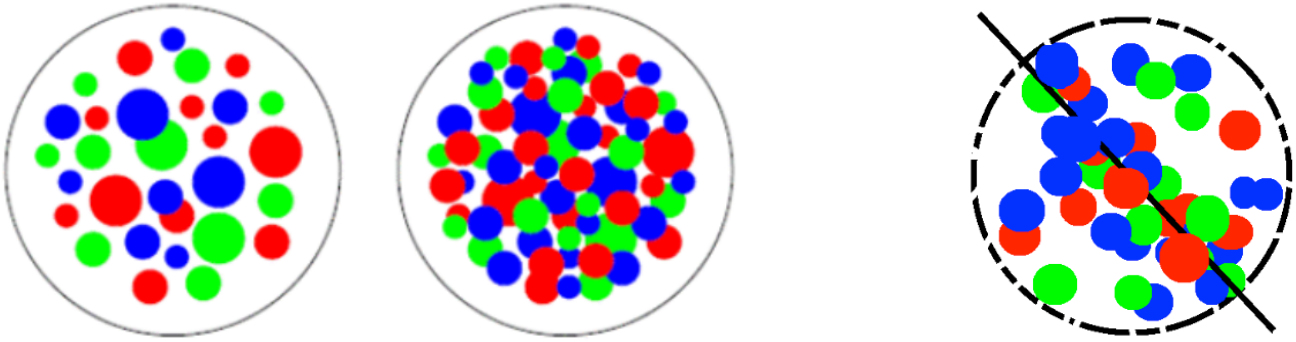

- Due to the random sum of the color charges in SU(3) the total charge decrease the particle multiplicity and gives an increase on the average tension of the strings
- A cluster of n strings that occupies an area Sn behaves as a single color source with a higher color field corresponding to a vectorial sum of color charges of each individual string

$$\vec{Q}_n^{\,2} = n\vec{Q}_1^{\,2} \longrightarrow \text{If strings are fully overlap}$$

$$\vec{Q}_n^{\,2} = n\frac{S_n}{S_1}\vec{Q}_1^{\,2} \longrightarrow \text{Partially overlap}$$

- The extended string between partons decays to new pairs of strings that latter form new partons which eventually hadronize (fragmentation). The particles are produce by the parton interactions via the Schwinger mechanism

Multiplicity and $\langle p_T^2 \rangle$ of particles produced by a cluster of n strings

multiplicity → $\frac{dn}{dy} \sim F(\xi)\bar{N}_s$

color reduction factor → $F(\xi) = \sqrt{\frac{1-e^{-\xi}}{\xi}}$

Number of strings → $N_p^s = 2 + 4\left(\frac{r_0}{R_p}\right)^2 \left(\frac{\sqrt{s}}{m_p}\right)^{2\lambda}$

string density in pp collisions → $\xi = N_p^s \left(\frac{r_0}{R_p}\right)^2$

$\lambda = .201$

proton mass

proton radius

M. A. Braun and C. Pajares, Eur. Phys. J. C16,349 (2000)
M. A. Braun et al, Phys. Rev. C65, 024907 (2002)

- The critical parameter is the string density

$$\xi = N_s \frac{S_1}{S_A},\ \xi_c = 1.1 - 1.5$$

- The area cover when one reach the critical densit $1 - e^{-\xi}$

- We assume that the cluster behaves like a single string but with higher color field and momentum

- In the large (n) limit the multiplicities and momentum sums:

$$< \mu_n >= \sqrt{\frac{nS_n}{S_1}} < \mu_1 > \ , < p_{Tn}^2 >= \sqrt{\frac{nS_1}{S_n}} < p_{T1}^2 >$$

Similar scaling laws are obtained for the product and the ratio of the multiplicities and transverse momentum in CGC

Both provide explanation for multiplicity suppression and $\langle p_T \rangle$ scaling with dN/dy.

Momentum Qs establishes the scale in CGC with the corresponding one in percolation of strings

The no. of color flux tubes in CGC and the effective no. of clusters of strings in percolation have the same dependence on the energy and centrality. (implications in Long range rapidity correlations and the ridge structure).

Clustering strings ~gluon saturation

$$Q_s^2 = \frac{k\langle p_T^2 \rangle_1}{F(\xi)}$$

$$Q_s^2 \sim \sqrt{(\xi)}$$

Y. V. Kovchegov, E. Levin, L. McLerran, Phys. Rev. C 63, 024903 (2001).
I. Bautista, J. Dias de Deus, C. Pajares, AIP Conf.Proc. 1343 (2011) 495-497

1. Multiplicity
2. p_T distribution
3. Particle ratios
4. Elliptic flow
5. Suppression of high pt particles RAA
6. J/ψ production
7. Forward -Backward Multiplicity Correlations at RHIC and LHC

Braun, Dias de Deus, Hirsch, Pajares, Scharenberg and Srivastava Phys. Rep. 599 (2015)

Properties of Small collision systems
QGP Droplet

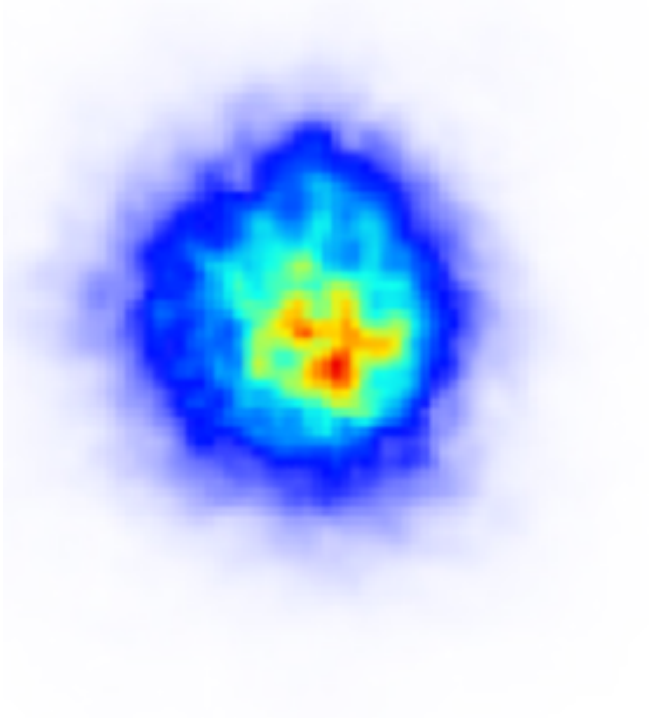

Thermodynamics on SPM

The model allows to relate concepts like temperature, entropy, and viscosity among other quantities as a function of the parameters

$$\zeta^t \ \& \ F(\zeta^t)$$

The Schwinger mechanism for no massive particles is given by:

$$\frac{dN}{dp_T} \sim e^{-\sqrt{2F(\zeta^t)}\frac{p_T}{\langle p_T \rangle_1}}$$

which can be related with the average value of the string tension of the strings $\langle x^2 \rangle = \pi \langle p_T^2 \rangle_1 / F(\zeta)$ These value fluctuates around its mean value since the chromo electric filed is not constant, and the fluctuations gives a Gaussian distribution of the string tension which can be seen as a thermal distribution.

$$T(\zeta^t) = \sqrt{\frac{\langle p_T^2 \rangle_1}{2F(\zeta^t)}}$$

H. G. Dosch, Phys. Lett. 190 (1987) 177 A. Bialas, Phys. Lett. B 466 (1999) 301

Power law for the transverse momentum distribution

$$\frac{d^2N}{dp_T^2} = \omega(\alpha, p_0, p_T) = \frac{(\alpha-1)(\alpha-2)}{2\pi p_0^2} \frac{p_0^\alpha}{[p_0+p_T]^\alpha}$$

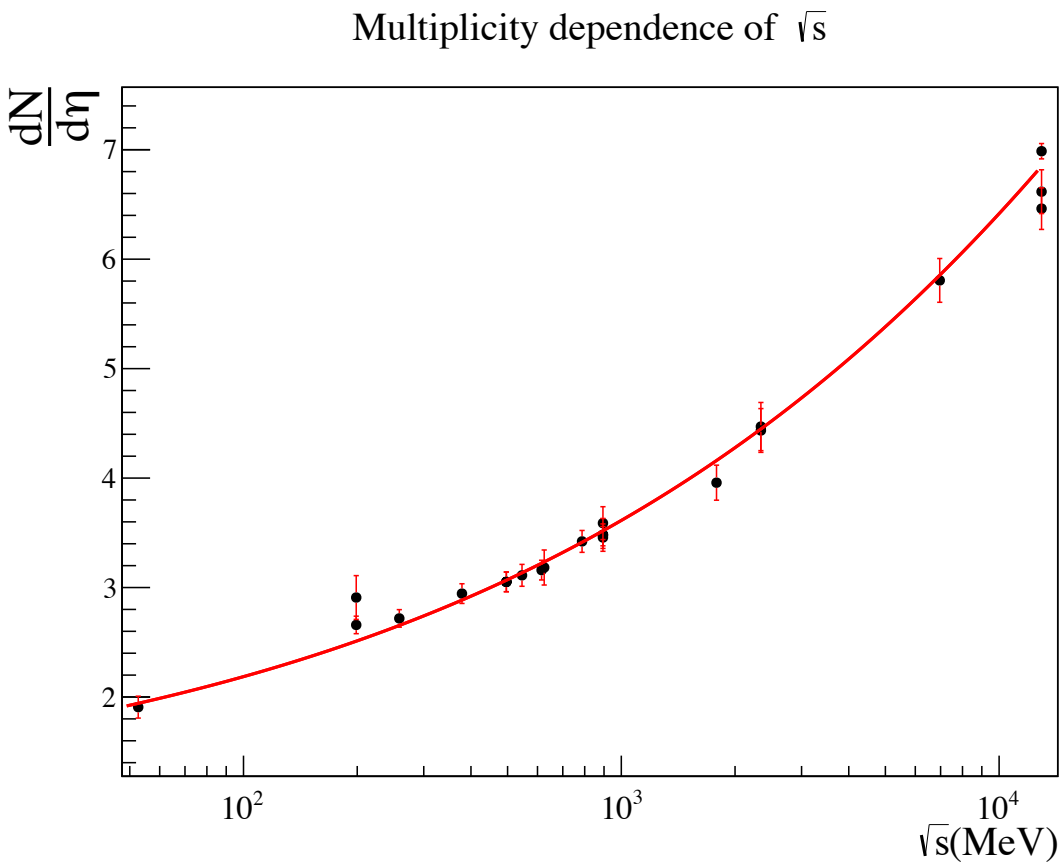

Nucl. Phys. A 698, 331 (2002)

I. Bautista, C. Pajares, J. G. Milhano and J. Dias de Deus, Phys. Rev. C **86** (2012) 034909

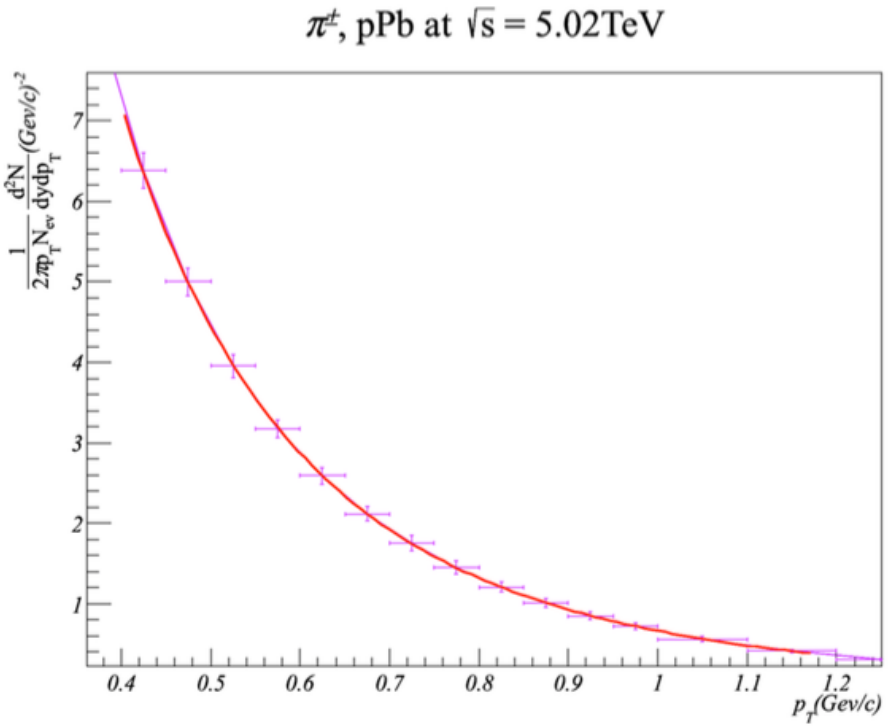

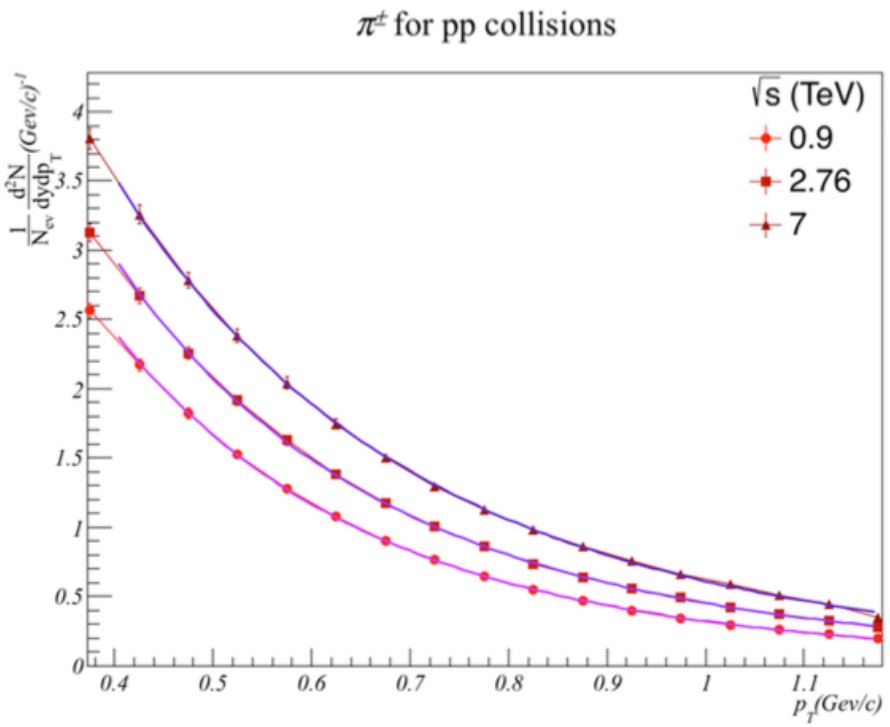

$\sqrt{S}(TeV)$	a	p_0	α
5.02	29.63±67.6	3.35±9.14	10.83±22.02
7	33.48±9.3	2.32±0.88	9.78±2.53
2.76	22.48±4.2	1.54±0.46	7.94±1.41
0.9	23.29±4.48	1.82±0.54	9.4±1.8

B. B. Abelev *et al.* [ALICE Collaboration], Eur. Phys. J. C **74** (2014) no.9, 3054

S. Chatrchyan *et al.* [CMS Collabora- tion], Eur. Phys. J. C **72**, 2164 (2012)

Power law for the transverse momentum distribution

$$\frac{d^2N}{dp_T^2} = \omega(\alpha, p_0, p_T) = \frac{(\alpha-1)(\alpha-2)}{2\pi p_0^2} \frac{p_0^\alpha}{[p_0+p_T]^\alpha}$$

$$\frac{d^2N}{dp_T^2} = \frac{(\alpha-1)(\alpha-2)(p_0\sqrt{\frac{F(\zeta_{pp})}{F(\zeta_{HM})}})^{\alpha-2}}{2\pi[p_0\sqrt{\frac{F(\zeta_{pp})}{F(\zeta_{HM})}}+p_T]^\alpha}$$

$$\frac{1}{N}\frac{d^2N}{d\eta dp_T} = a'(\sqrt{s})\frac{dN}{d\eta}\Big|^{pp}_{\eta=0}(\sqrt{s})\omega(\alpha, p_0, p_T) = \frac{a(p_0\frac{F(\zeta_{pp})}{F(\zeta_{HM})})^{\alpha-2}}{[p_0\sqrt{\frac{F(\zeta_{pp})}{F(\zeta_{HM})}}+p_T]^{\alpha-1}}$$

Nucl. Phys. A 698, 331 (2002)

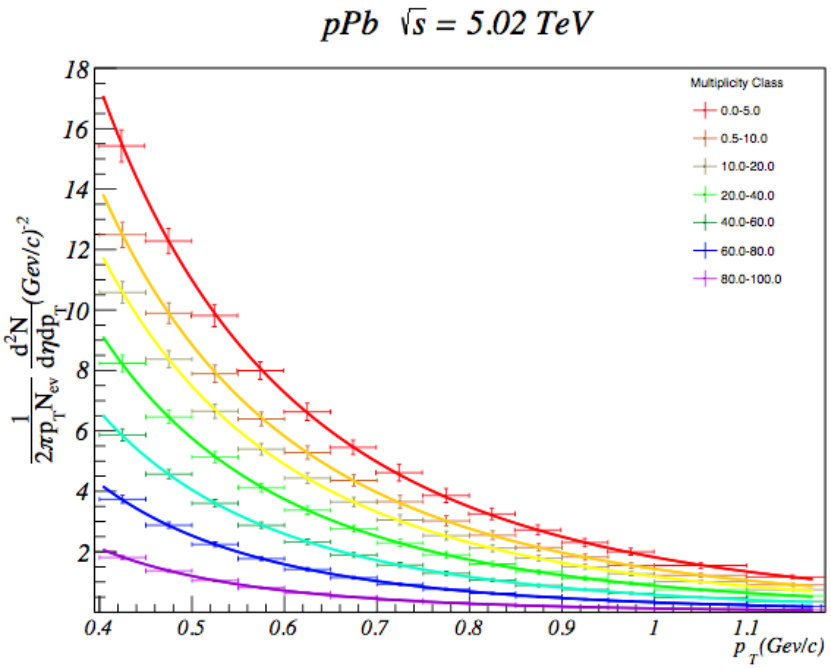

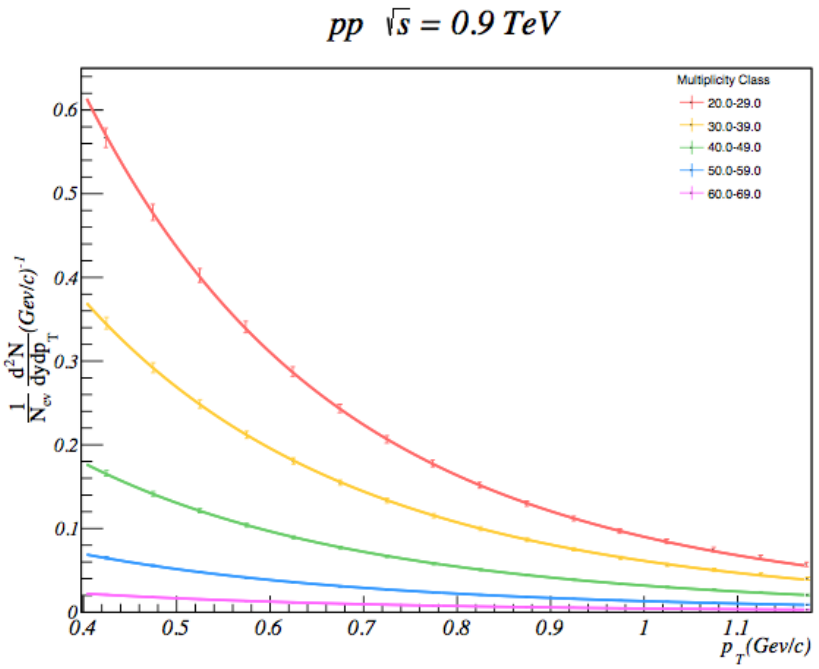

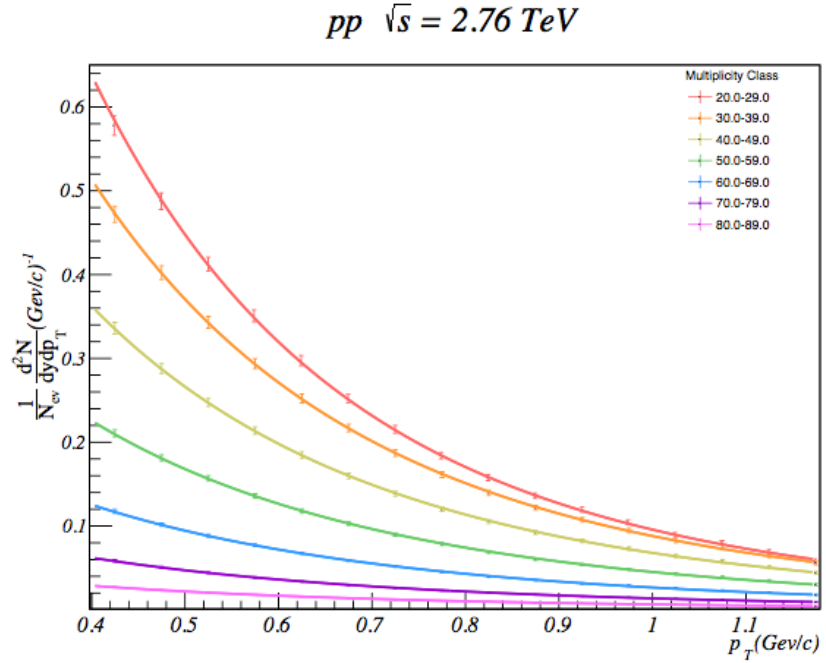

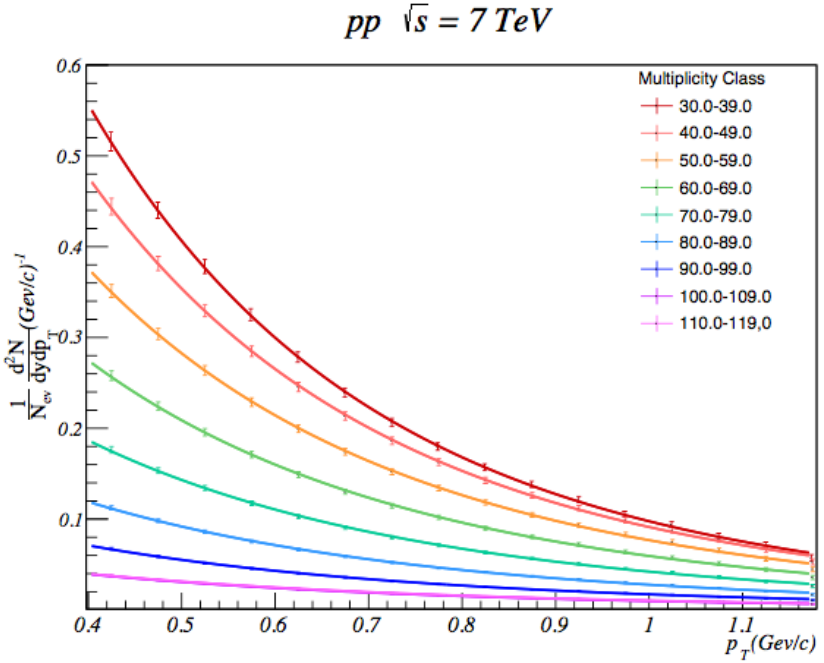

B. B. Abelev *et al.* [ALICE Collaboration], Eur. Phys. J. C **74** (2014) no.9, 3054

S. Chatrchyan *et al.* [CMS Collabora- tion], Eur. Phys. J. C **72**, 2164 (2012)

Color reduction factor

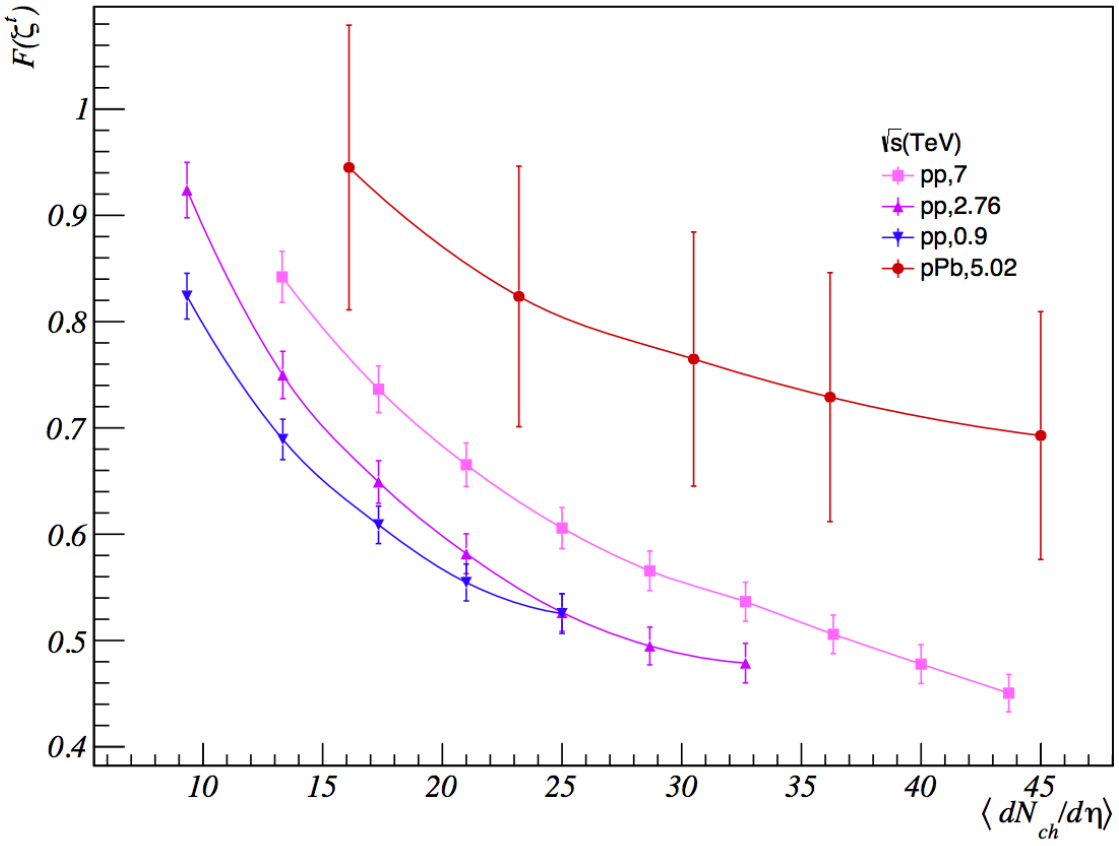

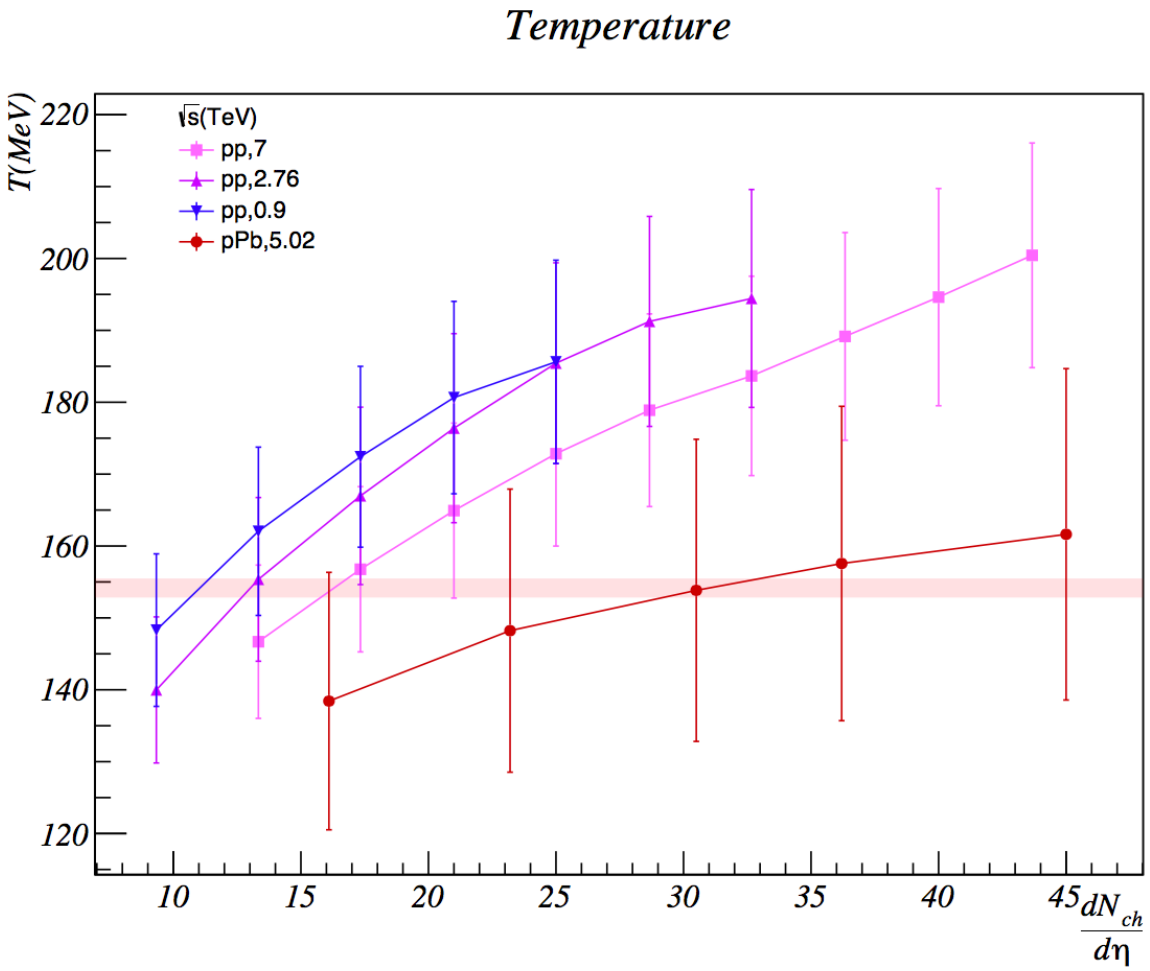
Temperature
T(MeV)
220
200
180
160
140
120
√s(TeV)
pp,7
pp,2.76
pp,0.9
pPb,5.02
10
15
20
25
30
35
40
45
dN_ch/dη

To fit data we use the scaling $1-e^{p(\mu)}$, where $p(\mu)$ is a polynomial in multiplicity considering a limit for very high multiplicities F_0 is the limit on saturation scale and we have a logarithmic dependence on the ratio of the energy over the threshold $\sim 1/\ln(s_0/s)$ of gluon saturation 2

$$F(\zeta^t) = F_0 + \frac{1 - \exp\left[\left(\frac{\mu}{\mu_0} + a_1\right)^{\frac{\sqrt{s}}{\sqrt{s_0}}}\right]}{a_0 \ln\left(\frac{\sqrt{s_0}}{\sqrt{s}}\right)}, \quad (1)$$

Fit over diferent classes of multiplicity

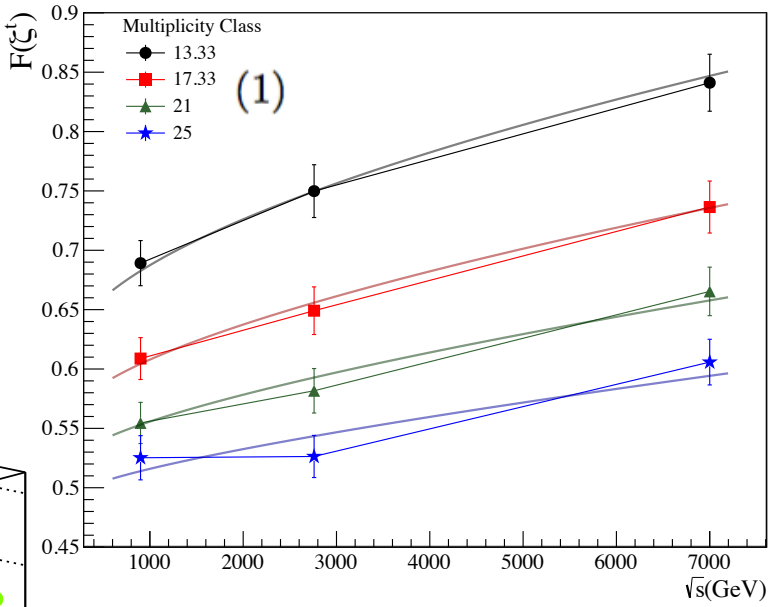

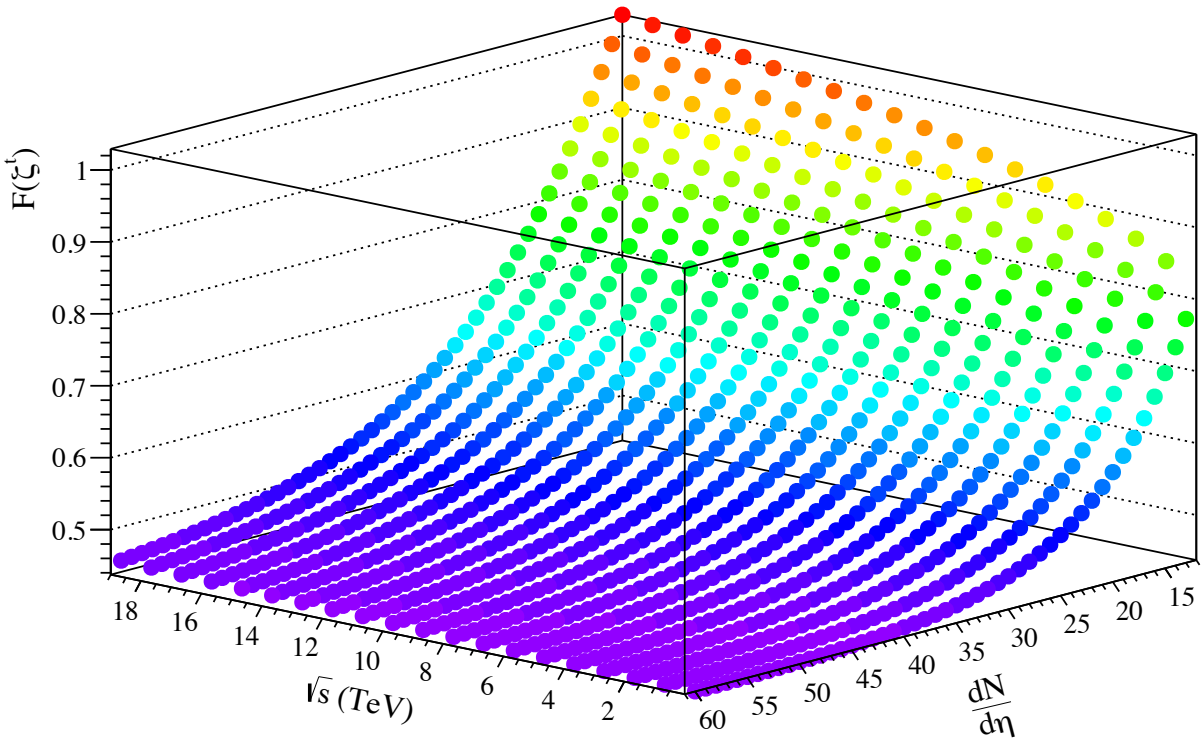

parameter	value	error
F_0	0.435241	0.0503243
$\sqrt{s_0}(\times 10^3 \text{TeV})$	1.40030	1.49161
μ_0	54.468	16.2556
a_1	0.00258187	0.00470024
a_0	0.119777262	0.026209073
a_0^{-1}	8.34883	1.82685

How small is the droplet?

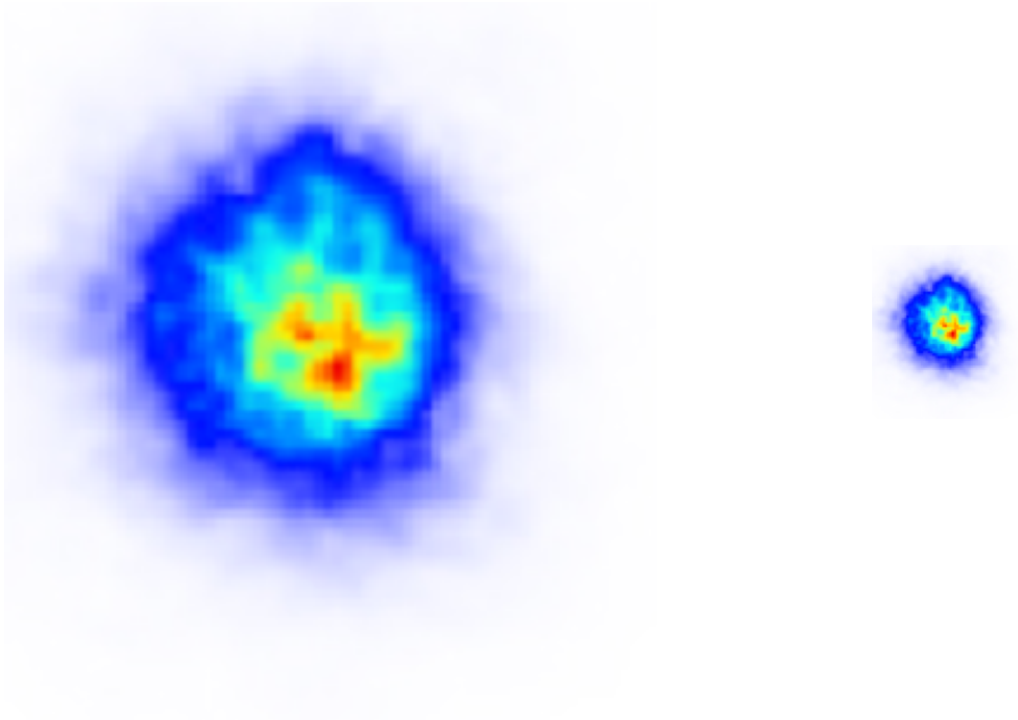

Monte Carlo

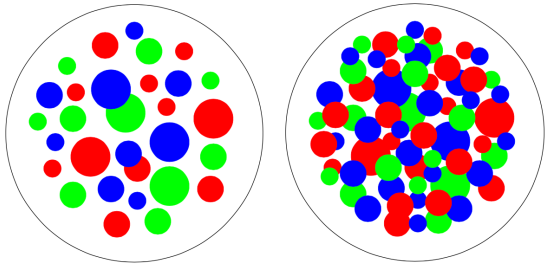

$$\varepsilon = \sqrt{1 - \frac{b^2}{a^2}}$$

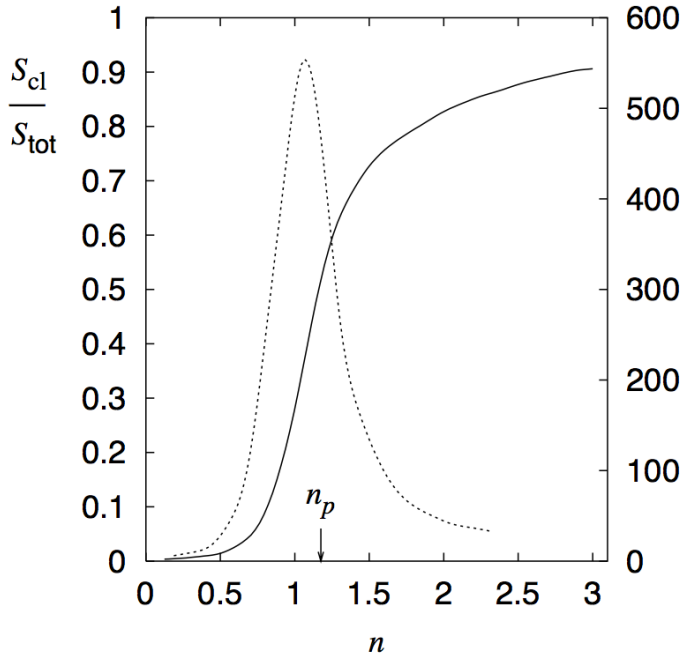

$$\eta = \frac{r_0^2 N}{ab}. \qquad a^2 = \frac{r_0^2 N}{\eta\sqrt{1-\varepsilon^2}}; \qquad b^2 = \frac{r_0^2 N\sqrt{1-\varepsilon^2}}{\eta}$$

Once determined a and b, we take a random point (x, y) distributed in the rectangle $[-(a - r_0), a - r_0] \times [-(b - r_0), b - r_0]$ according with a density profile. This point is the center of the string and it is included in the string population if satisfies the following condition

$$\frac{x^2}{(a - r_0)^2} + \frac{y^2}{(b - r_0)^2} \leq 1.$$

The constrictions will only consider strings completely embedded in the elliptical region. In this way, we can generate all N strings needed to build the percolating system. Note that with this construction, in the limit $\varepsilon = 0$, we recover the particular case for a SPM bounded by circles, which has been already studied by several authors

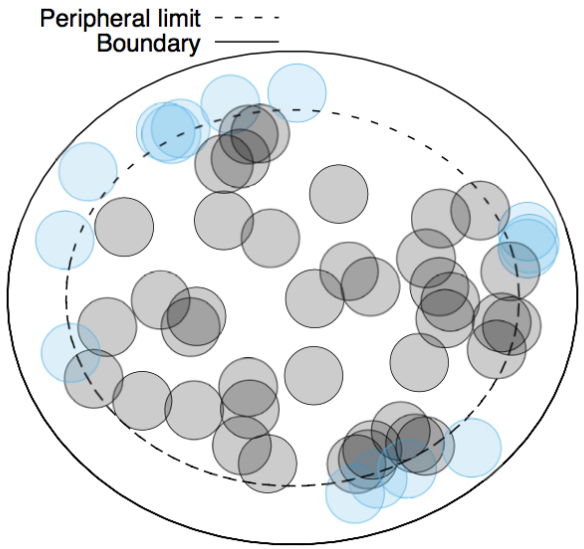

The solid line is the elliptic boundary of the system and the dashed line represents the internal peripheral limit needed to define a spanning cluster. Blue circles are the peripheral strings satisfying the relation

$$\frac{x^2}{(a-2r_0)^2} + \frac{y^2}{(b-2r_0)^2} > 1.$$

In this way, we assure that there is a spanning cluster in the string system if the largest cluster has more than one peripheral string and the largest distance between the peripheral strings is greater than $2(b - 2r_0)$. This ensure that the spanning cluster at least cross-over the system through the minor semi-axes.

Density Profiles

$$f(x,y) = \frac{1}{2\pi\sigma_a\sigma_b}\exp\left[-\frac{1}{2}\left(\frac{x^2}{\sigma_a^2}+\frac{y^2}{\sigma_b^2}\right)\right]:$$

$$\sigma_a = (a-r_0), \quad \sigma_b = (b-r_0);$$
$$\sigma_a = (a-r_0)/2^{1/2}, \quad \sigma_b = (b-r_0)/2^{1/2};$$
$$\sigma_a = (a-r_0)/2, \quad \sigma_b = (b-r_0)/2.$$

σ_a and σ_b are standard deviations over the semi-axis of the ellipse

$1s$, $2^{1/2}s$ y $2s$

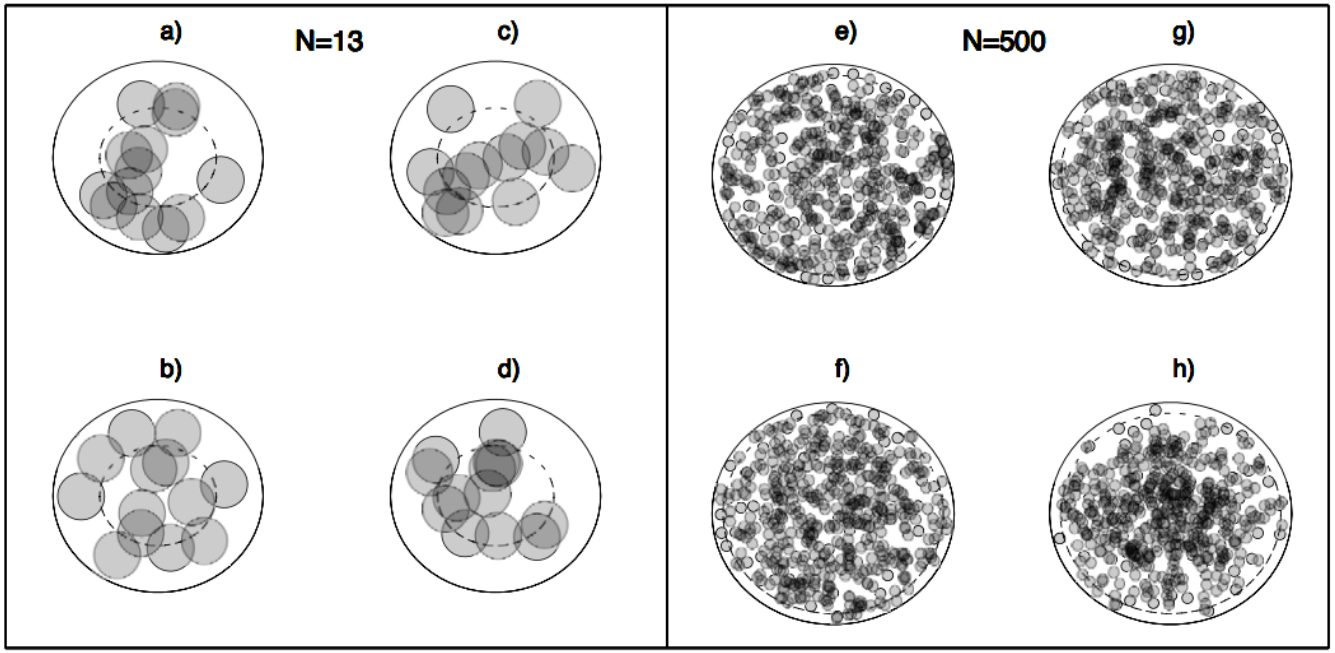

Samples of a percolating system for different density profiles. Left box: String systems at $N = 13$, $\eta = 0.7$ and $\varepsilon = 0.4$, for the models a) Uniform, b) $1s$, c) $2^{1/2}s$ and d) $2s$; Right box: String systems at $N = 500$, $\eta = 1.1$ and $\varepsilon = 0.4$, for the models e) Uniform, f) $1s$, g) $2^{1/2}s$ and h) $2s$.

String percolation threshold for elliptically bounded systems, I. Bautista, A. Fernández. J. E Ramirez, Physica 488 (2017) 8-15.

Among profiles there is not much differences but we expect to have larger differences as we increase the number of strings.

As the number of peripheral discs decrease the percolation threshold becomes higher

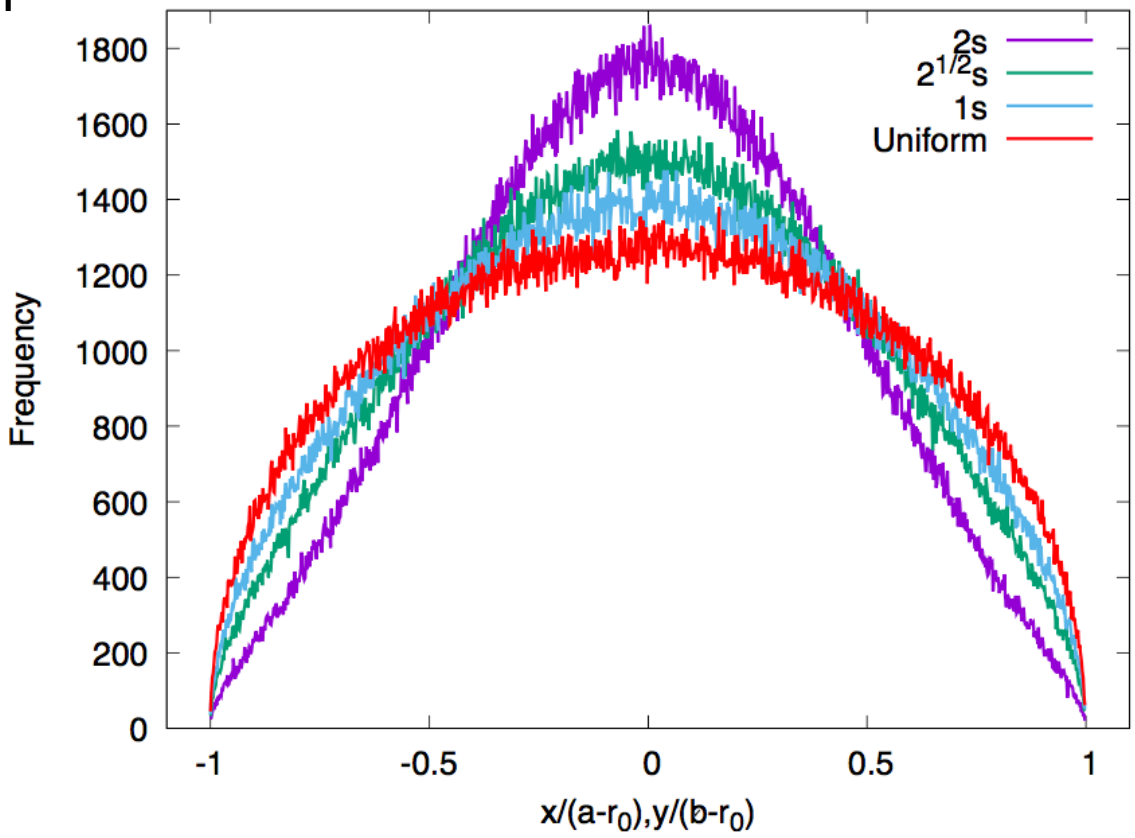

Projection of the disc position distribution over the axis of the ellipse for the different profile functions. The histograms were built with a 10^6 generated positions for each model. The distributions are normalized to the semi-axis value to eliminate the dependence on the number of discs N, ε and η.

String percolation threshold for elliptically bounded systems, I. Bautista, A. Fernández. J. E Ramirez, Physica 488 (2017) 8-15.

The percolation threshold appears when the derivative ∂P/∂η takes its maximum value

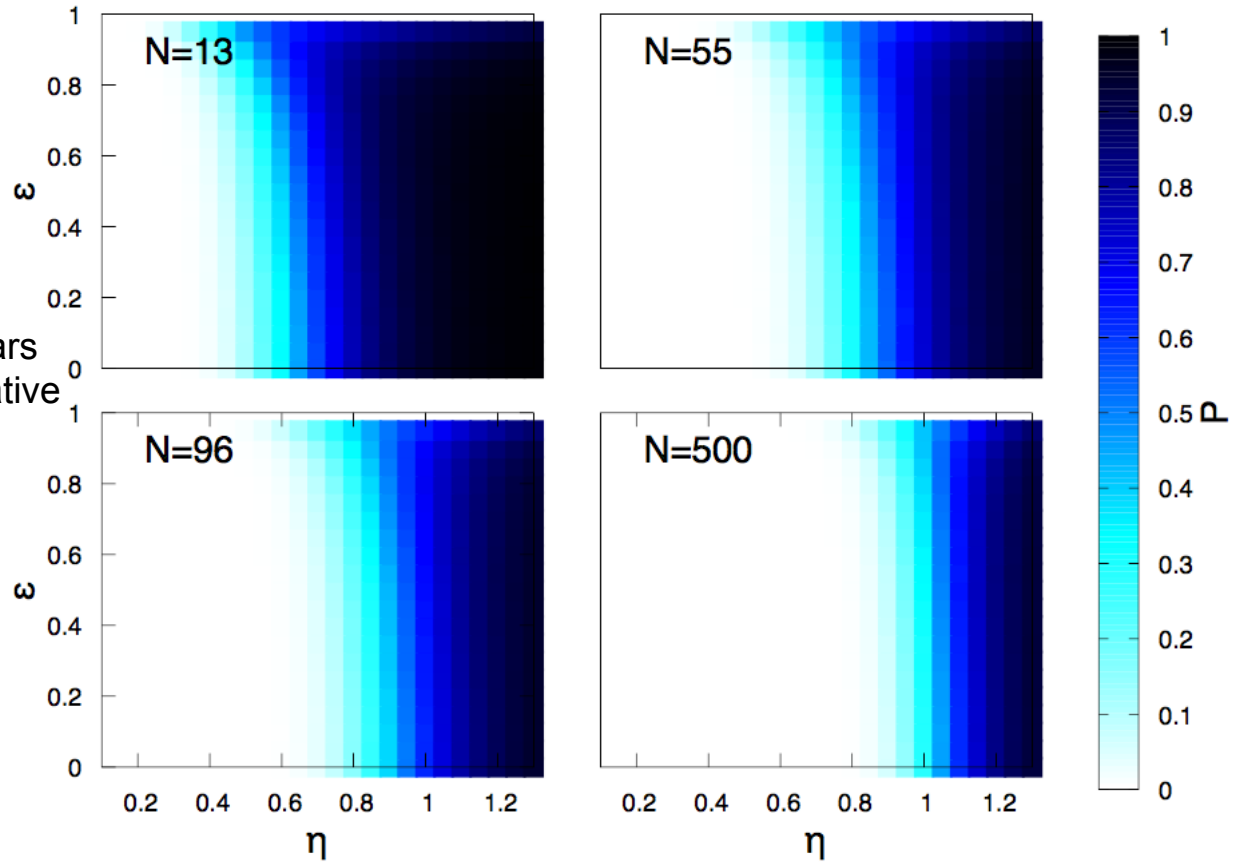

The percolation probability shows an evident shift as a function of N and high eccentricity dependence associated with a finite size effect.

Percolation probability P as a function of filling factor η and eccentricity ε for different values of a number of strings N with Uniform density profile.

For largest values of N, the percolation probability becomes independent of the eccentricity and the phase transition appears around the percolation threshold for the continuum percolation in the thermodynamic limit.

String percolation threshold for elliptically bounded systems, I. Bautista, A. Fernández. J. E Ramirez, Physica 488 (2017) 8-15.

$$P(\eta) = \frac{1}{1 + \exp\left(-\sum_{k=0}^{4} a_k \eta^k\right)}$$

the fraction of occupied/connected sites belonging to the spanning cluster

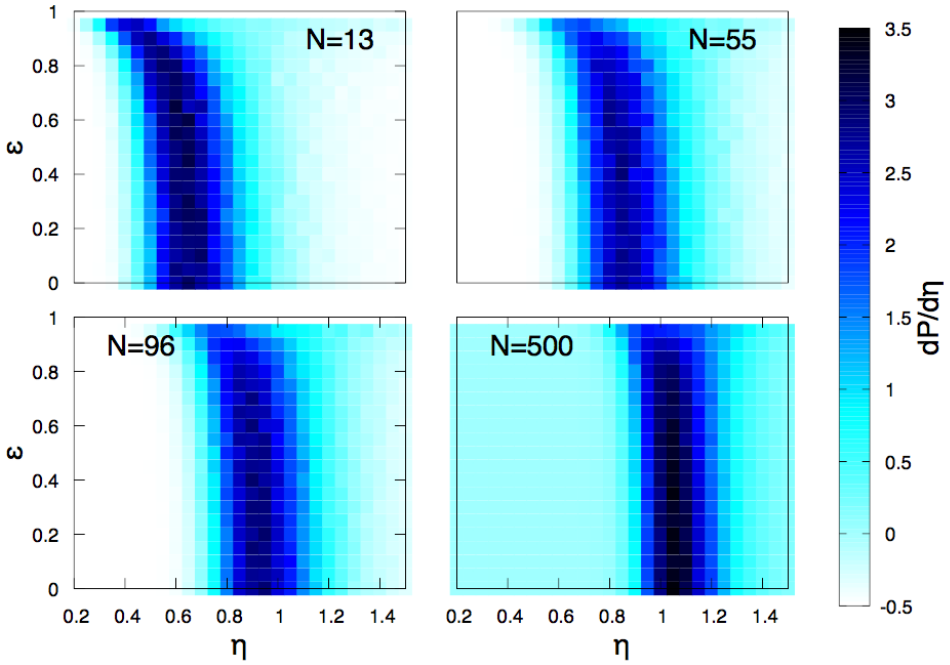

A derivative of the percolation probability with respect to filling factor η in the Uniform model.

To obtain the value of η_c, the equation $P(\eta_c) = 0.5$ has to be solved. However, for N = 500 and the model with Gaussian density profiles, we use

$$P(\eta) = \frac{1}{2}\left[1 + \tanh\left(\frac{\eta - \eta_c}{\Delta L}\right)\right]$$

where η_c is the percolation threshold and ΔL is the width of the percolation transition. In Fig. 7, we show the best fit obtained for the percolation probability as a function of filling factor for different values of η and N in string percolating systems with Uniform density profile

String percolation threshold for elliptically bounded systems, I. Bautista, A. Fernández. J. E Ramirez, Physica 488 (2017) 8-15.

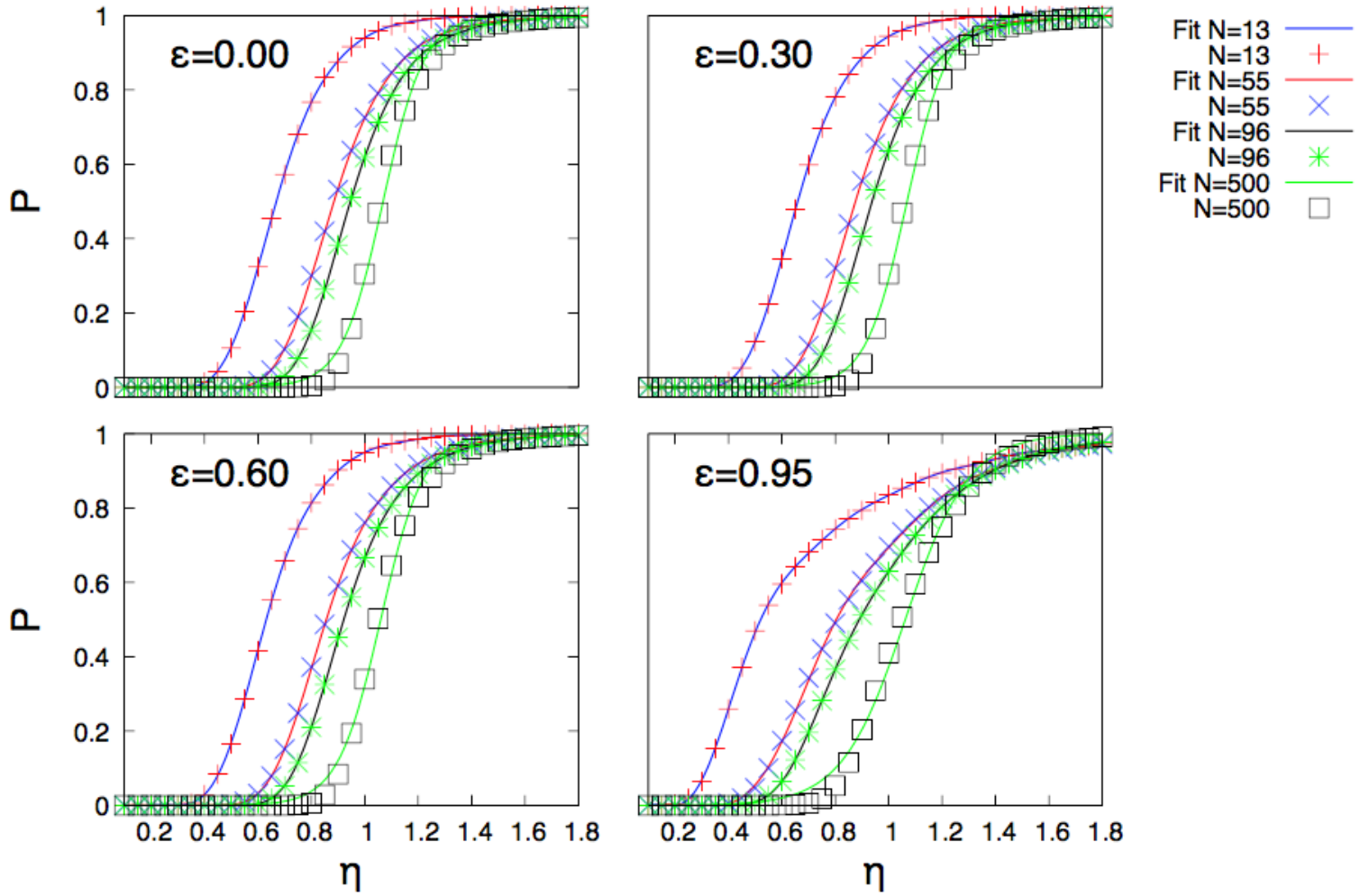

String percolation threshold for elliptically bounded systems, I. Bautista, A. Fernández. J. E Ramirez, Physica 488 (2017) 8-15.

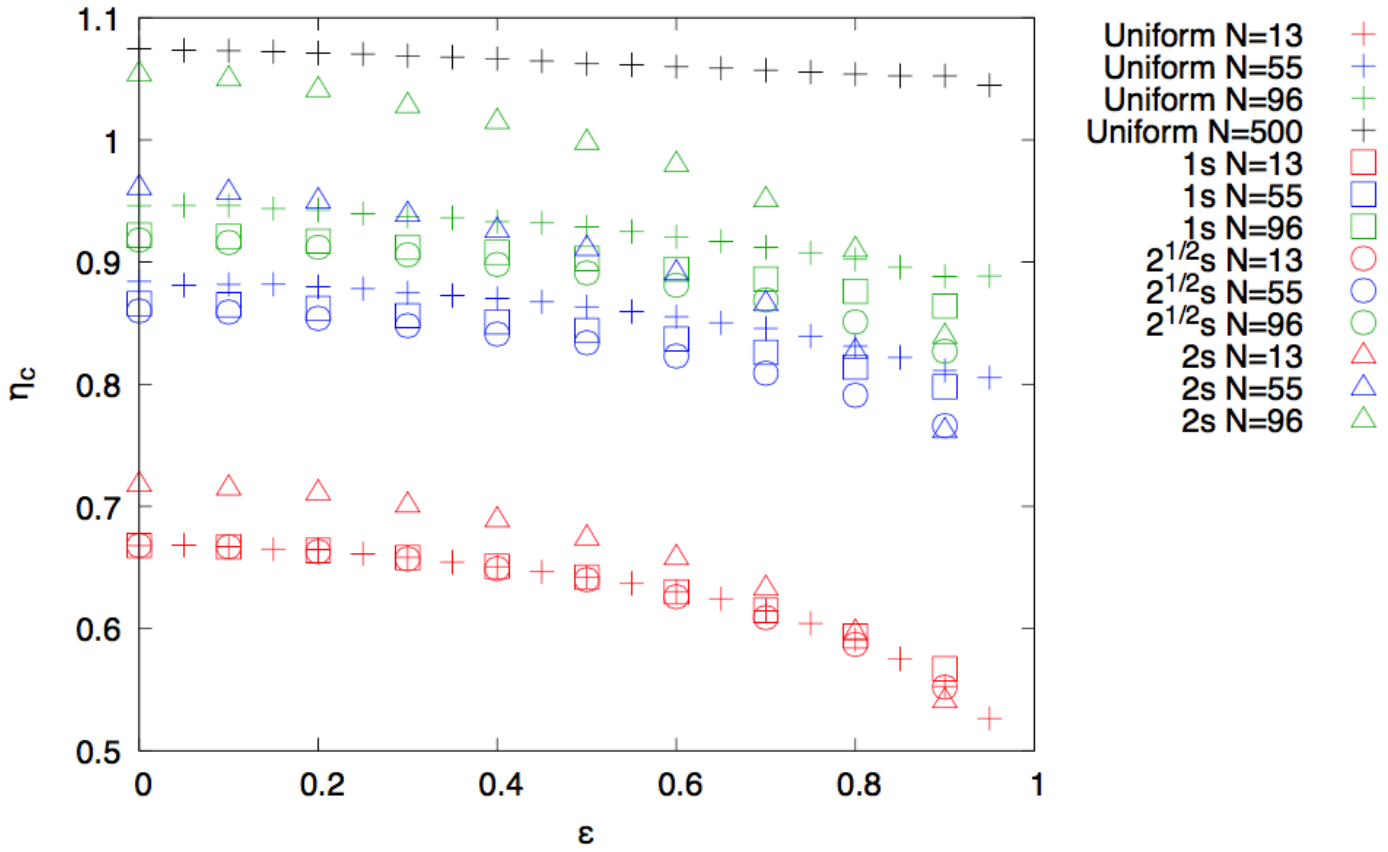

Percolation threshold η_c as a function of eccentricity (ε) for different values of N with the different density profiles: Uniform (crosses), and Gaussian: $1s$ (squares), $2^{1/2}s$ (circles) and $2s$ (triangles).

String percolation threshold for elliptically bounded systems, I. Bautista, A. Fernández. J. E Ramirez, Physica 488 (2017) 8-15.

How far from the thermodynamic limit?

$$\frac{\eta}{1-\exp(-\eta)} \equiv \frac{1}{F^2(\eta)} \longrightarrow \mu = N_S F(\eta)\mu_1 \; ; \; \langle p_{\rm T}^2 \rangle = \langle p_{\rm T}^2 \rangle_1 / F(\eta)$$

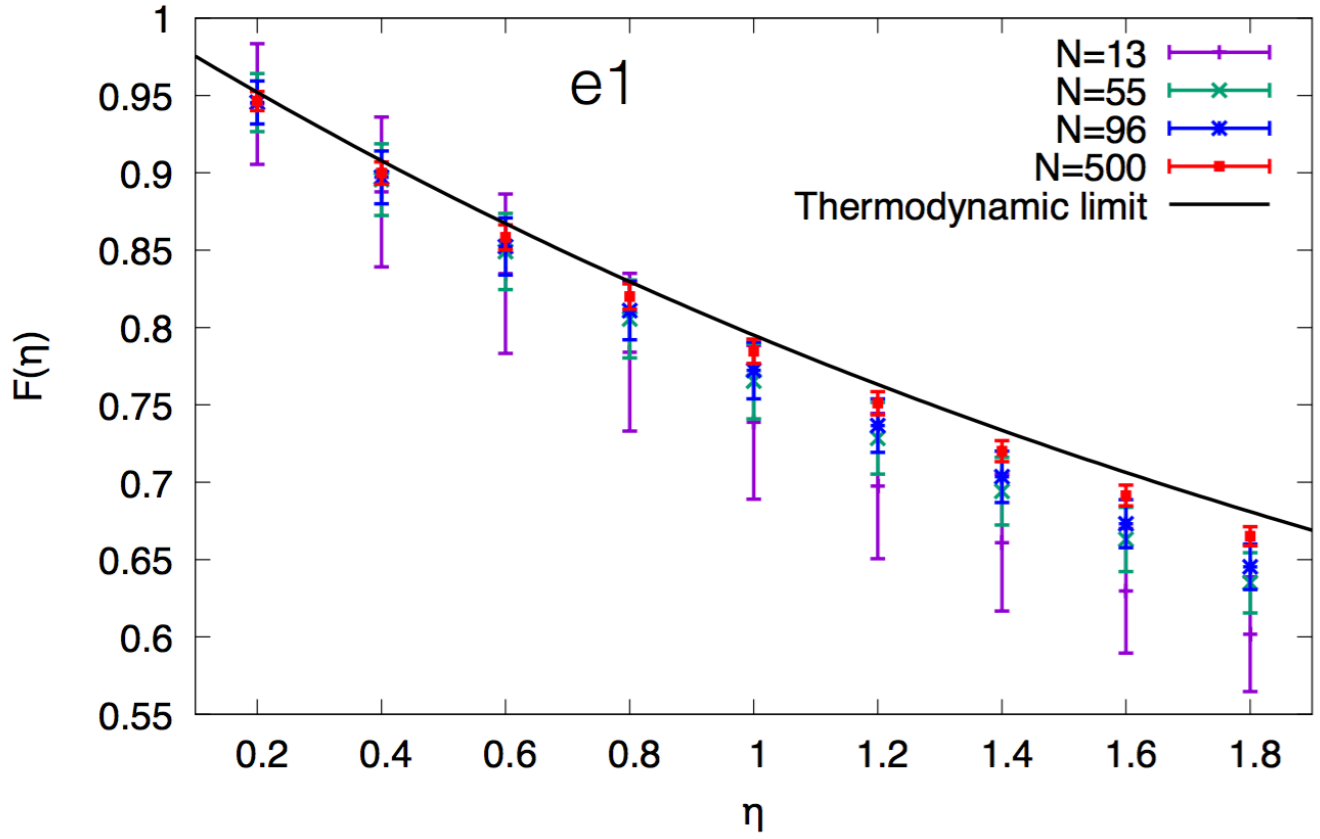

Initial geometry fluctuations of the droplet?

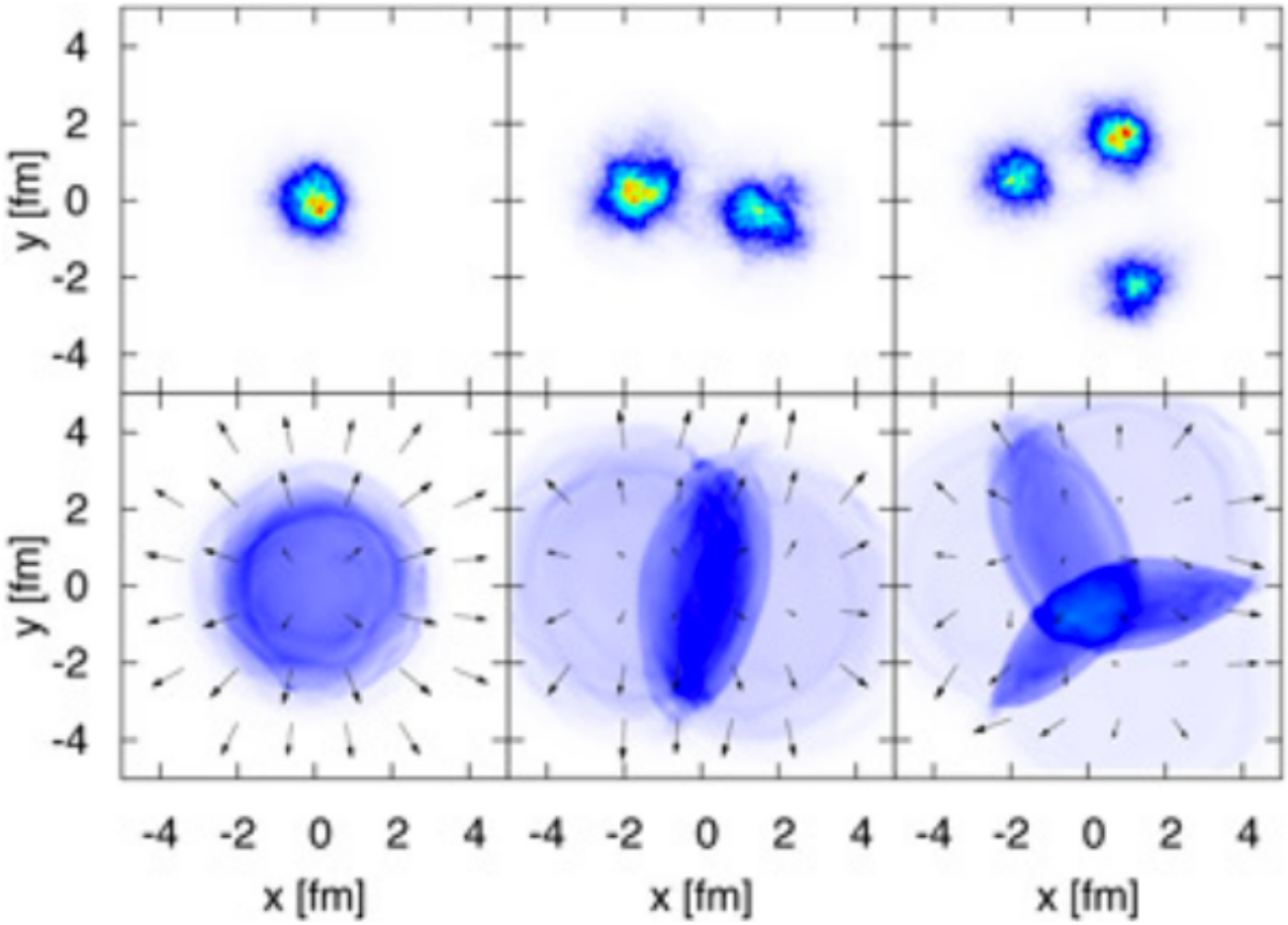

Image taken from Bjoern Schenke The Drops of Early Universe Perfect Fluid, Brookhaven Newsroom

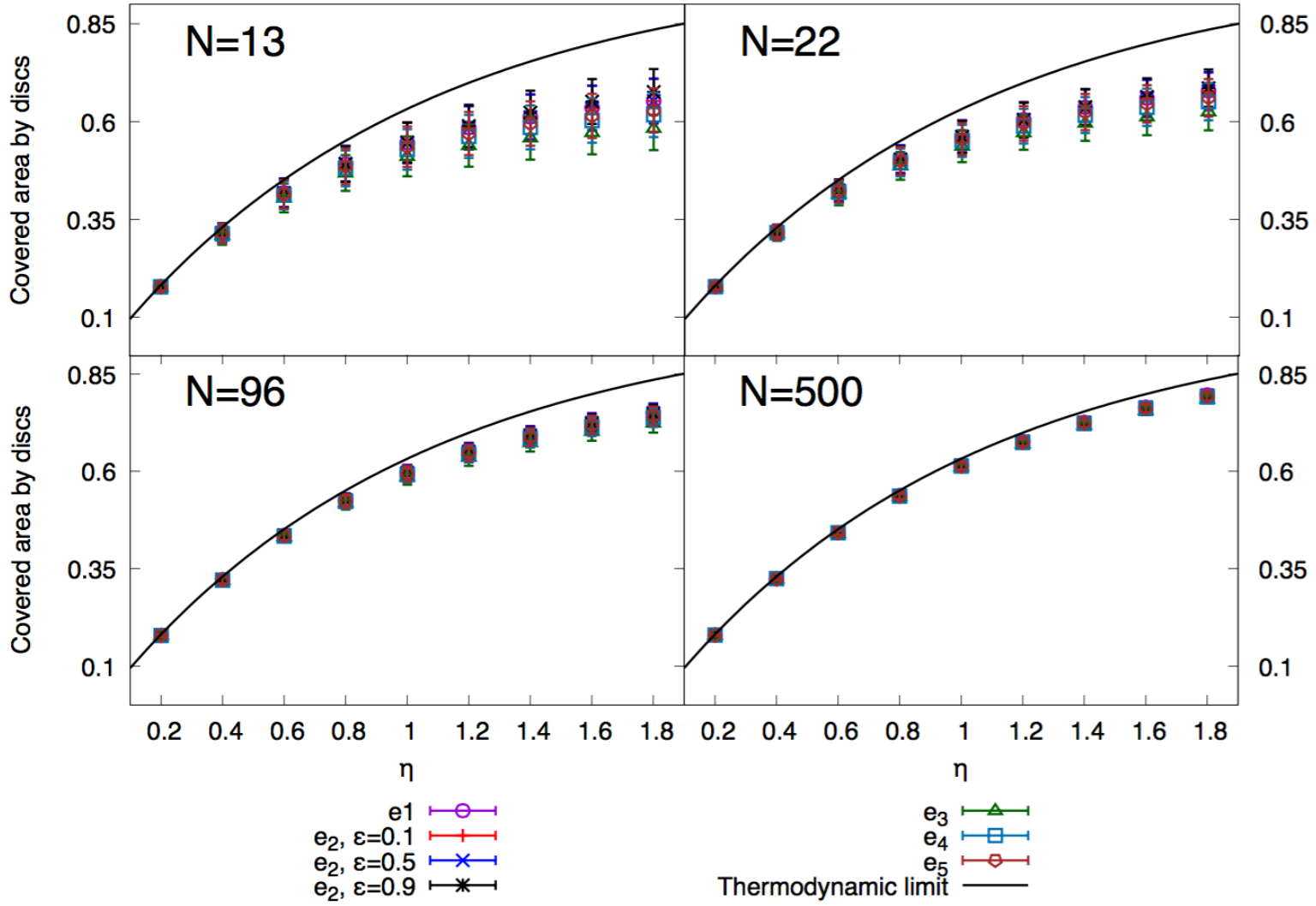
N=13
N=22
N=96
N=500
Covered area by discs
Covered area by discs
0.85
0.6
0.35
0.1
0.2
0.4
0.6
0.8
1
1.2
1.4
1.6
1.8
η
η
e1
e2, ε=0.1
e2, ε=0.5
e2, ε=0.9
e3
e4
e5
Thermodynamic limit

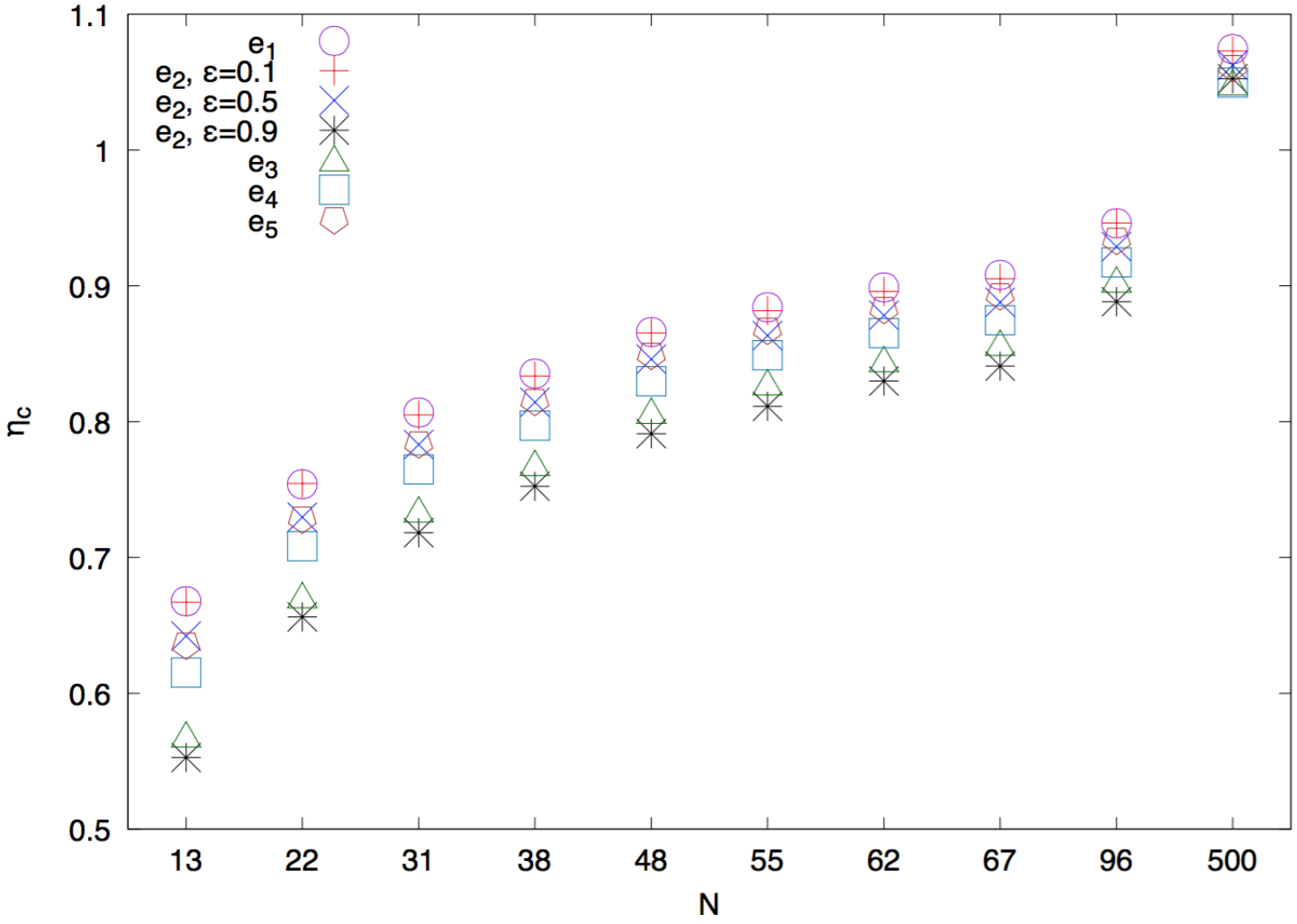
1.1
1
0.9
0.8
0.7
0.6
0.5
η_c
13
22
31
38
48
55
62
67
96
500
N
e_1
e_2, ε=0.1
e_2, ε=0.5
e_2, ε=0.9
e_3
e_4
e_5

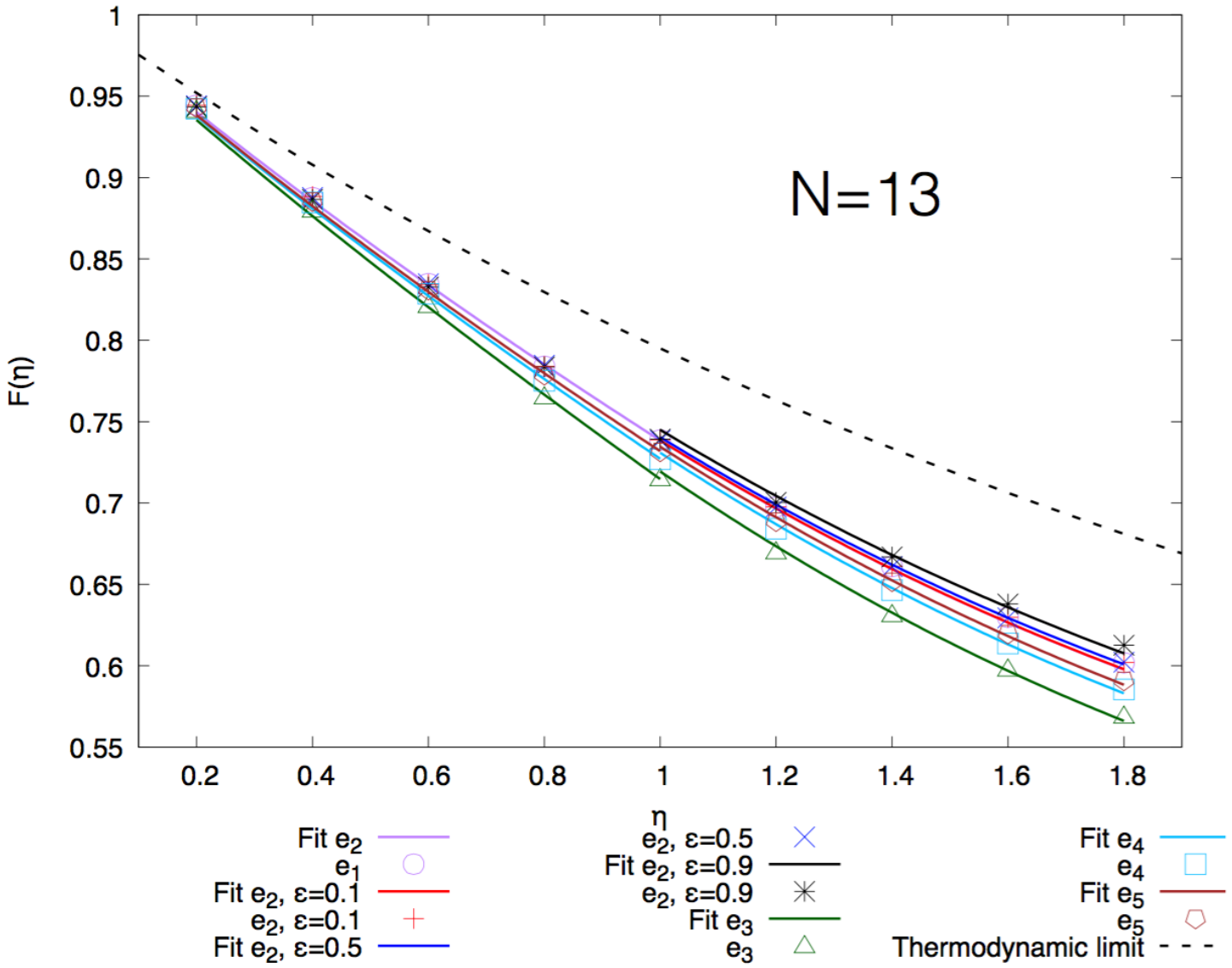
N=13
F(η)
η
1
0.95
0.9
0.85
0.8
0.75
0.7
0.65
0.6
0.55
0.2
0.4
0.6
0.8
1
1.2
1.4
1.6
1.8
Fit e2
e1
Fit e2, ε=0.1
e2, ε=0.1
Fit e2, ε=0.5
e2, ε=0.5
Fit e2, ε=0.9
e2, ε=0.9
Fit e3
e3
Fit e4
e4
Fit e5
e5
Thermodynamic limit

Elliptic Flow: A collective effect

Beam's eye view of a non-central collision:

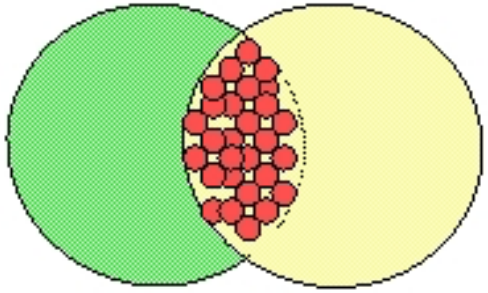

Particles prefer to be "in plane":

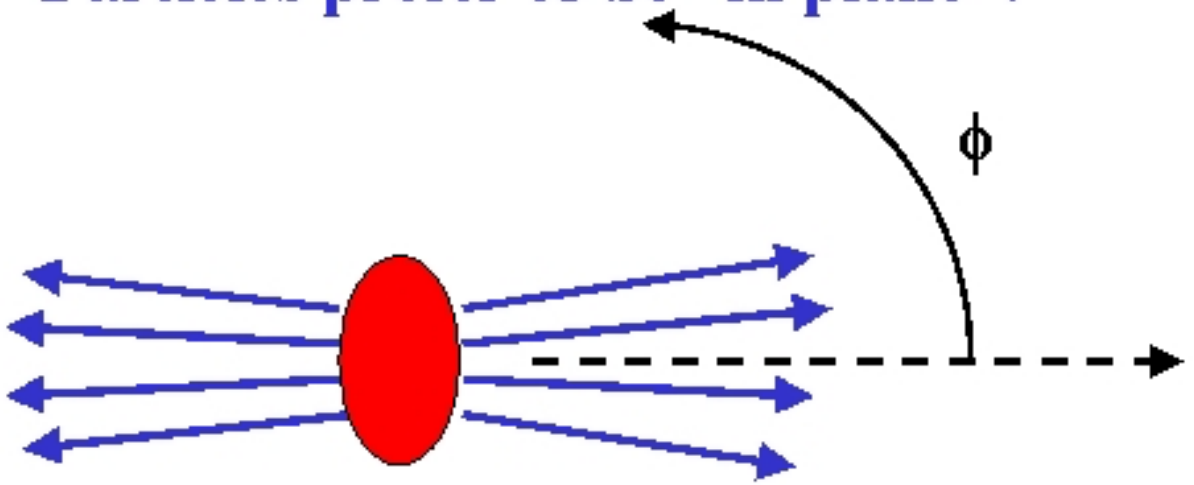

$$dN/d(\phi - \Psi_R) = N_0 (1 + 2V_1 \cos(\phi - \Psi_R) + 2V_2 \cos(2(\phi - \Psi_R)) + \dots)$$

Elliptic flow

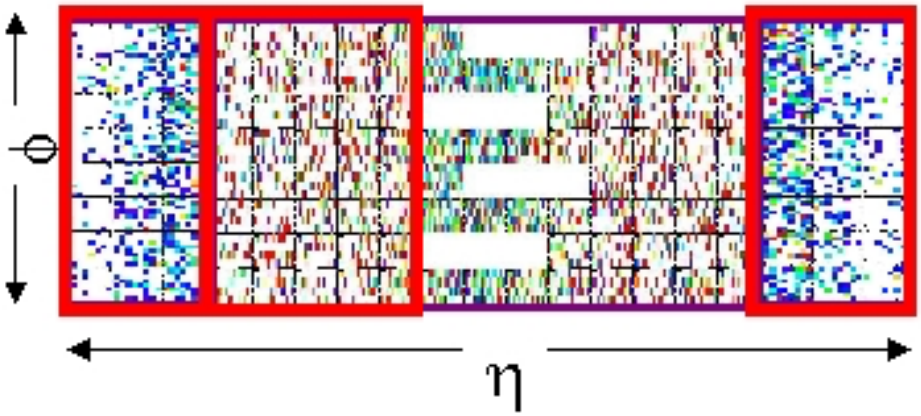

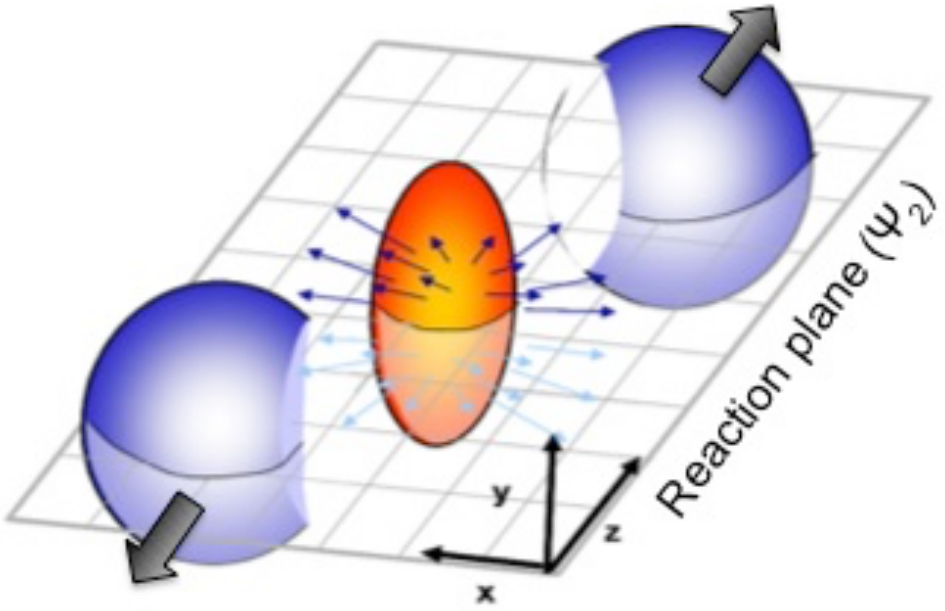

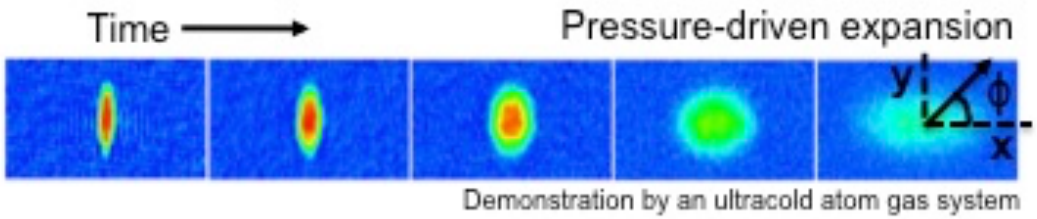

Demonstration by an ultracold atom gas system

Anisotropic azimuthal distribution:

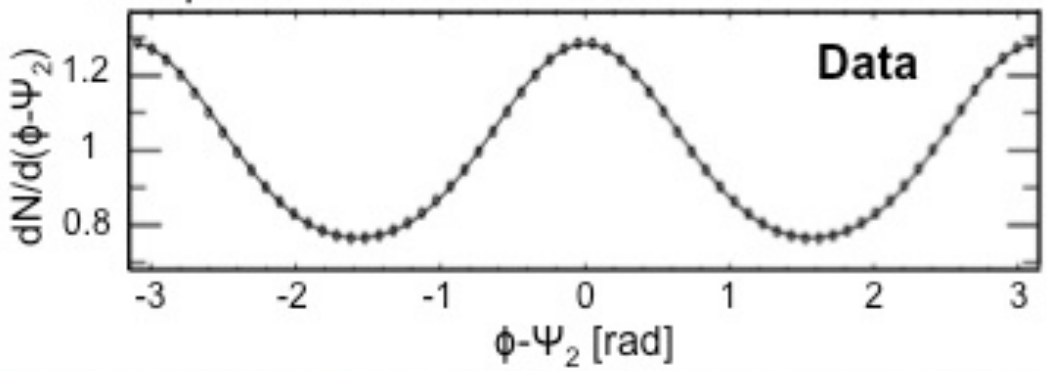

$dN/d(\phi-\Psi_2) \sim 1+2v_2\cos[2(\phi-\Psi_2)]$ v_2: elliptic flow

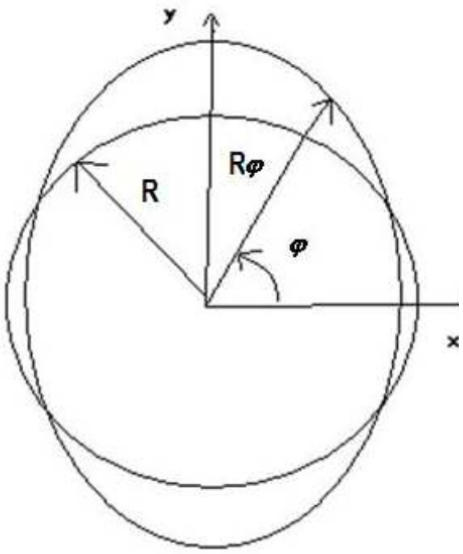

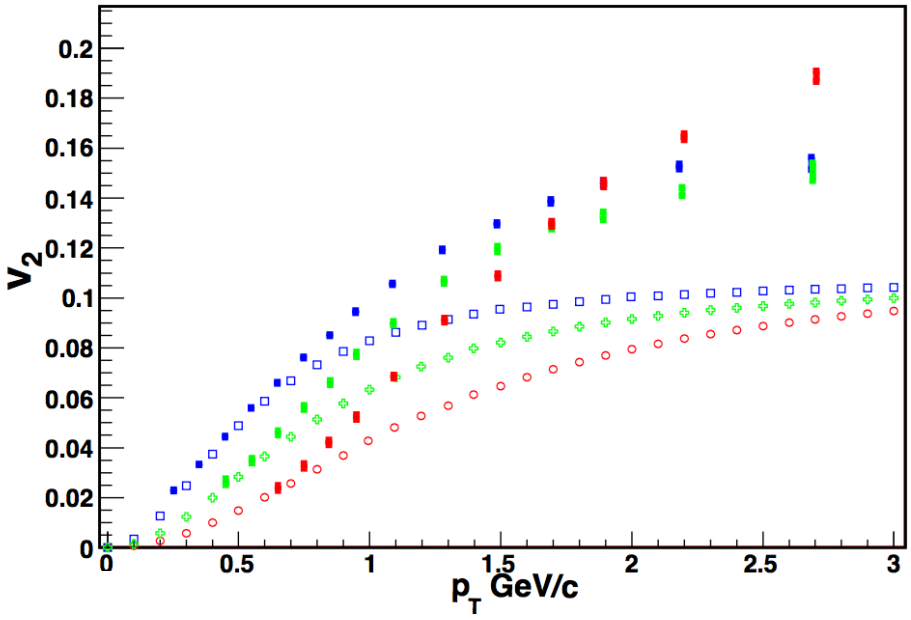

Figure 2: Elliptic flow for different hadron species in Au+Au coll
lines in red, blue and green show our predictions, for antiprotons, pions and kaons respectively, dashed lines experimental data from RHIC [48].

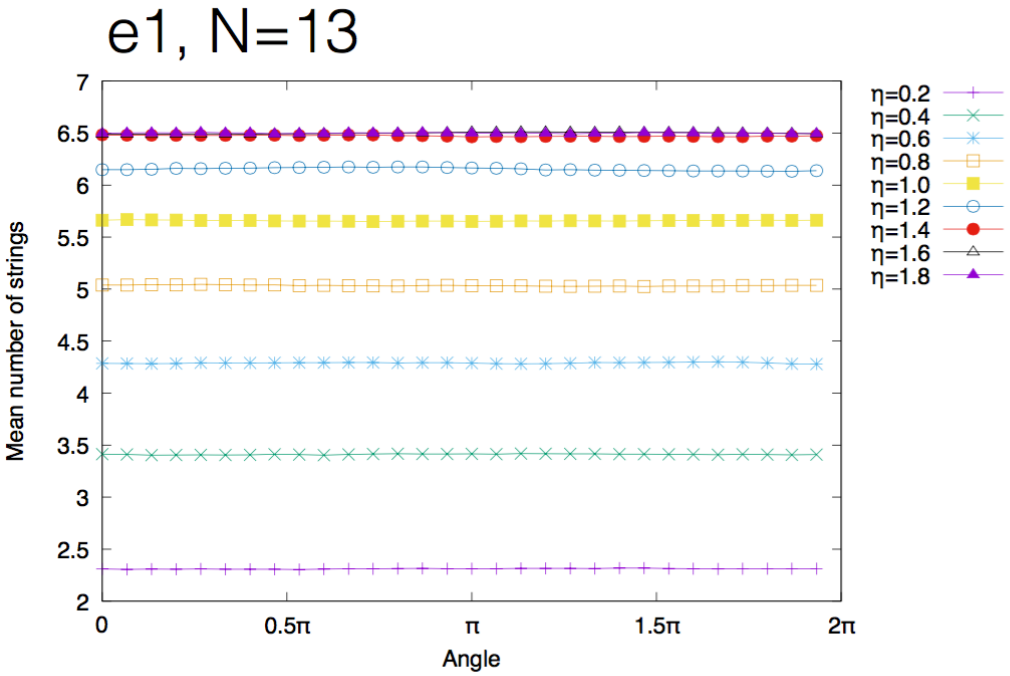
e1, N=13
Mean number of strings
Angle
7
6.5
6
5.5
5
4.5
4
3.5
3
2.5
2
0
0.5π
π
1.5π
2π
η=0.2
η=0.4
η=0.6
η=0.8
η=1.0
η=1.2
η=1.4
η=1.6
η=1.8

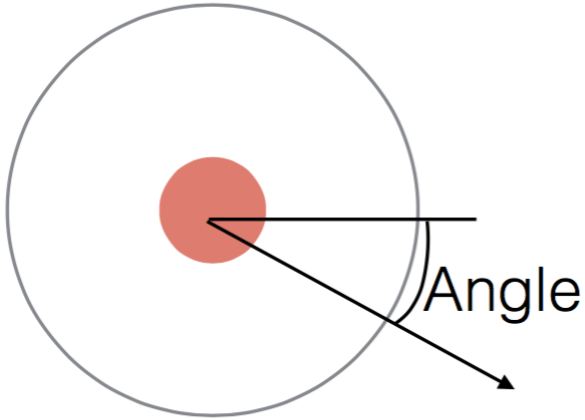
Angle

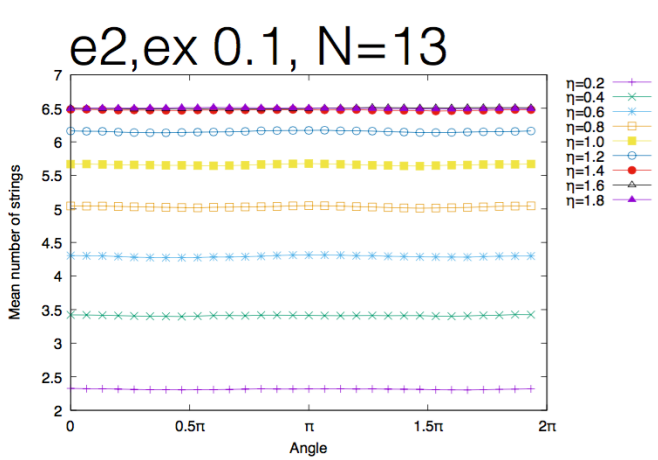
e2,ex 0.1, N=13
Mean number of strings
Angle
0
0.5π
π
1.5π
2π
η=0.2
η=0.4
η=0.6
η=0.8
η=1.0
η=1.2
η=1.4
η=1.6
η=1.8

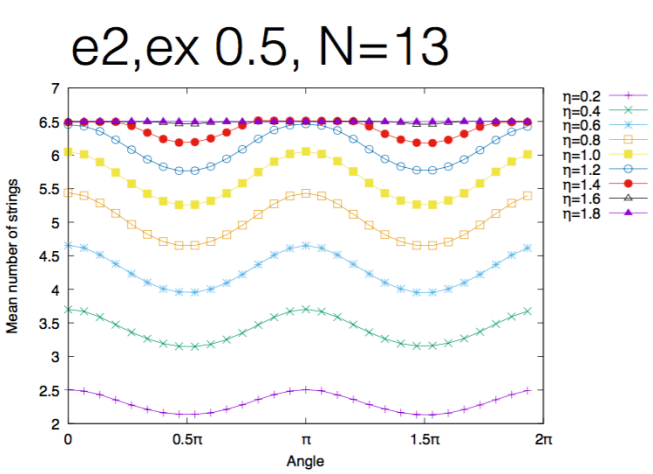
e2,ex 0.5, N=13
Mean number of strings
Angle
0
0.5π
π
1.5π
2π
η=0.2
η=0.4
η=0.6
η=0.8
η=1.0
η=1.2
η=1.4
η=1.6
η=1.8

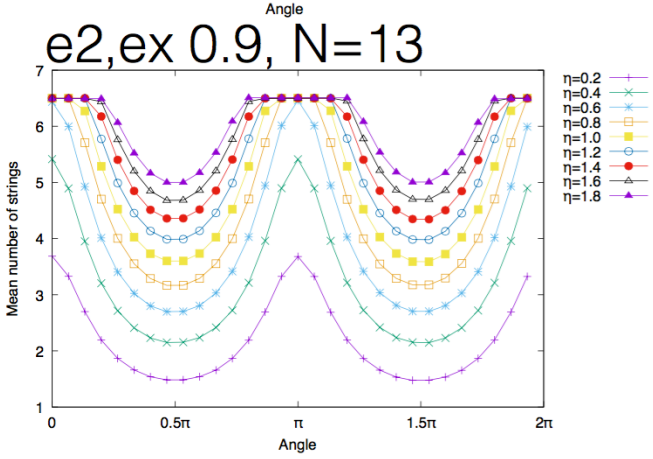
e2,ex 0.9, N=13
Mean number of strings
Angle
0
0.5π
π
1.5π
2π
η=0.2
η=0.4
η=0.6
η=0.8
η=1.0
η=1.2
η=1.4
η=1.6
η=1.8

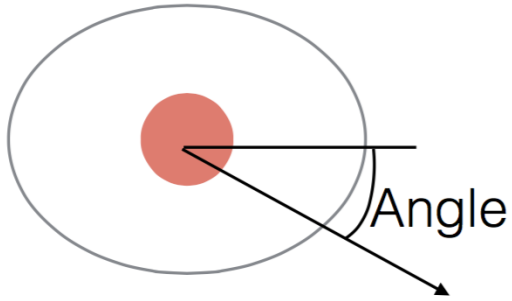
Angle

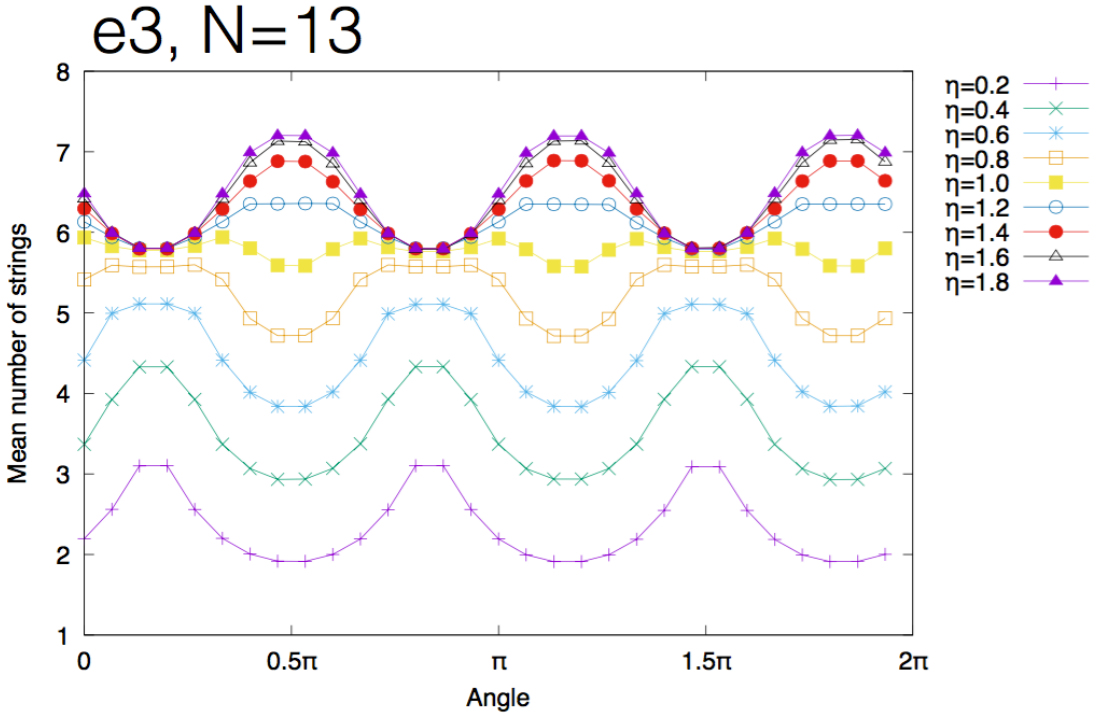
e3, N=13
Mean number of strings
Angle
0
0.5π
π
1.5π
2π
1
2
3
4
5
6
7
8
η=0.2
η=0.4
η=0.6
η=0.8
η=1.0
η=1.2
η=1.4
η=1.6
η=1.8

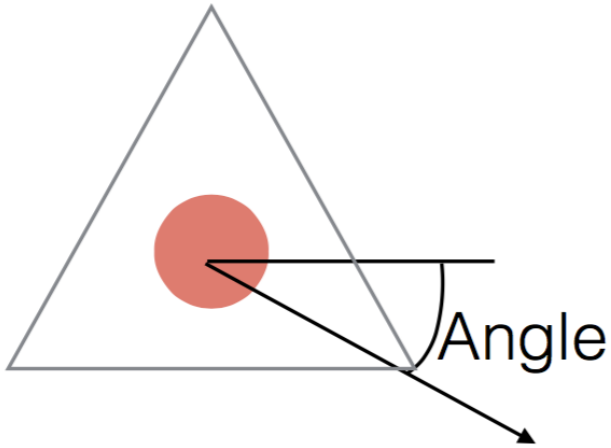
Angle

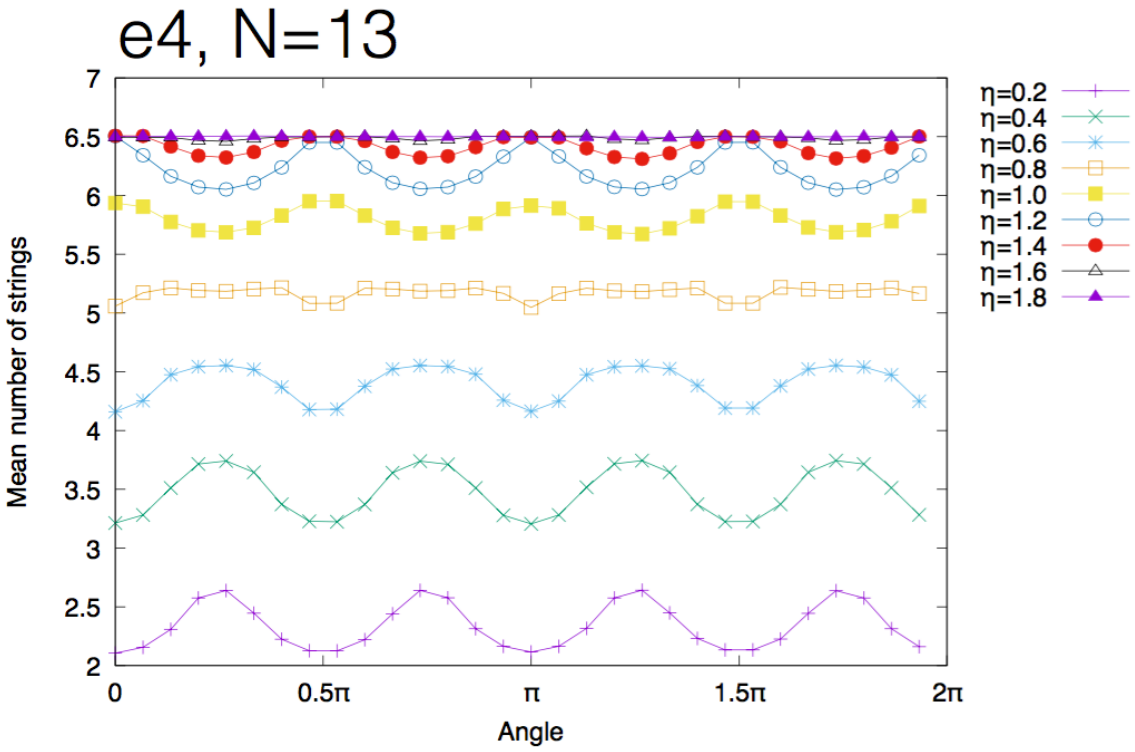
e4, N=13
Mean number of strings
Angle
7
6.5
6
5.5
5
4.5
4
3.5
3
2.5
2
0
0.5π
π
1.5π
2π
η=0.2
η=0.4
η=0.6
η=0.8
η=1.0
η=1.2
η=1.4
η=1.6
η=1.8

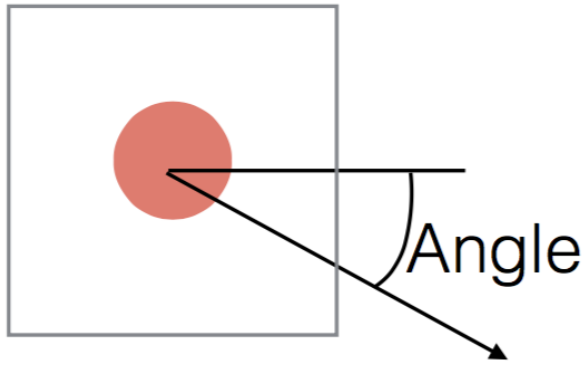
Angle

e5, N=13

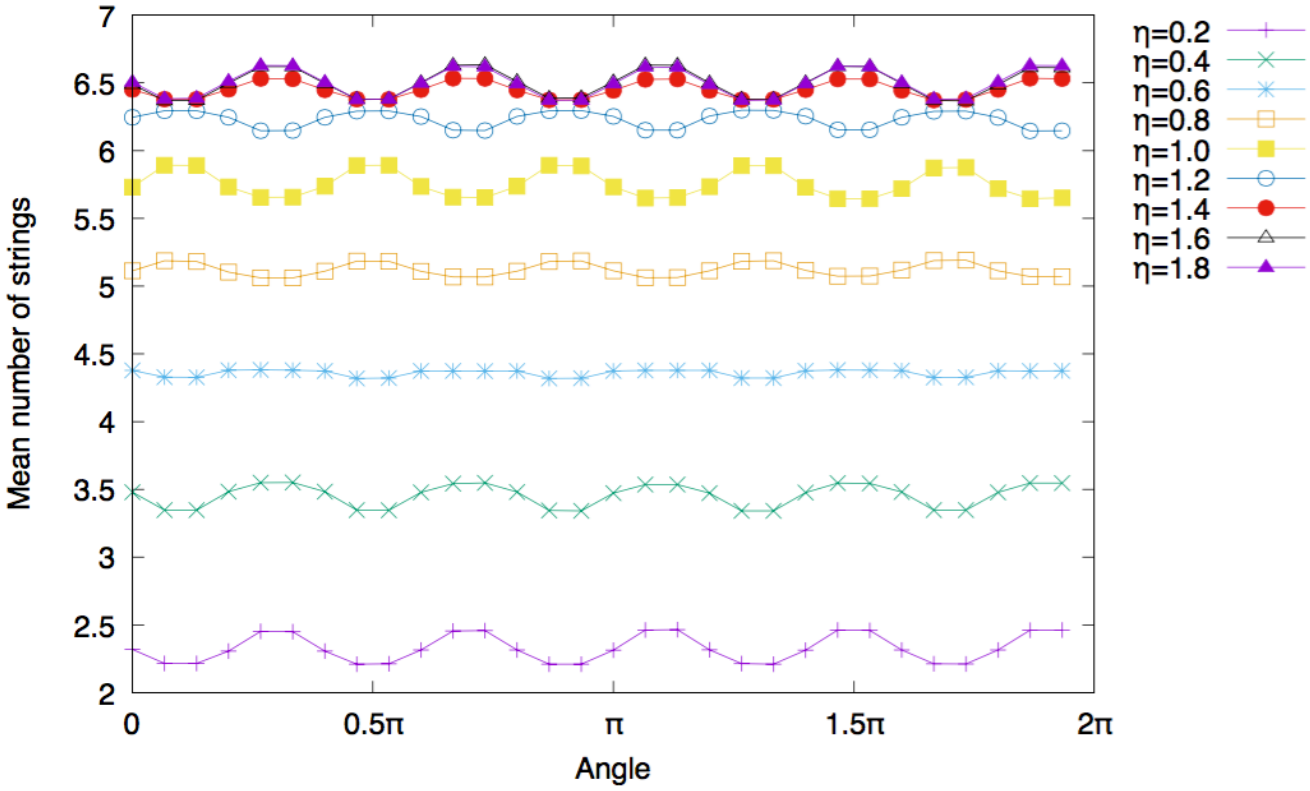
Mean number of strings
7
6.5
6
5.5
5
4.5
4
3.5
3
2.5
2
0
0.5π
π
1.5π
2π
Angle
η=0.2
η=0.4
η=0.6
η=0.8
η=1.0
η=1.2
η=1.4
η=1.6
η=1.8

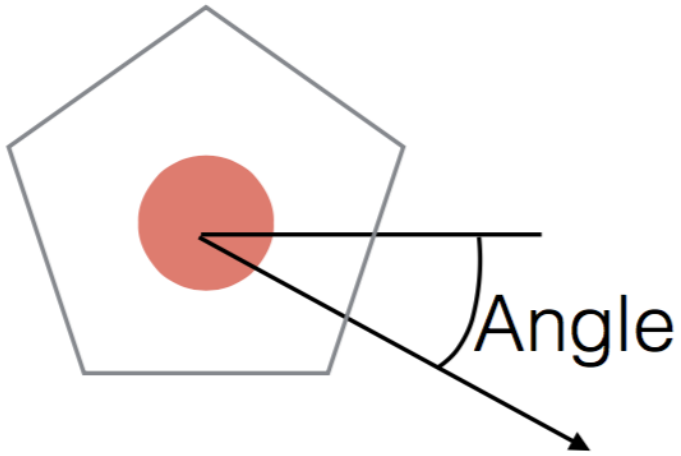
Angle

Now we can relate the particle production for the different initial geometry modes that are shown in the above figure to calculate the contribution due to geometry fluctuation of the initial anisotropy ε_n defined in a similar manner as in reference *

$$\varepsilon_n = \varepsilon_n e^{in\varphi_n} = \frac{\int r^n e^{n\varphi} \zeta^t(r,\varphi) r dr d\varphi}{\int r^n \zeta^t(r,\varphi) r dr d\varphi}$$

Where ζ^t is the transverse string density, and with the usual polar coordinates in the transverse plane.

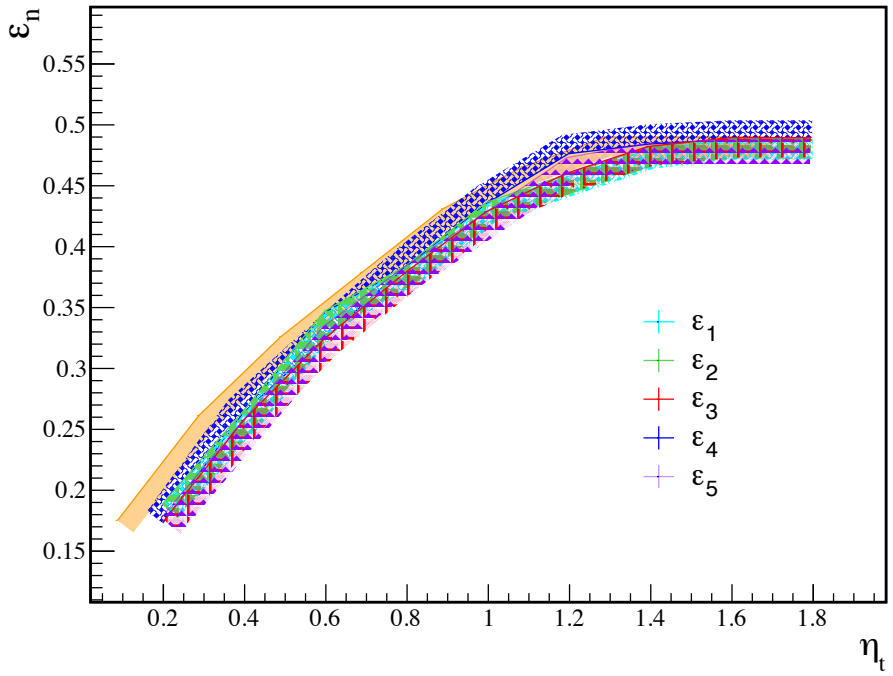

* L. Yan, J. Y. Ollitrault and A. M. Poskanzer, Phys. Lett. B 742 (2015) 290.

What else can we study?

Correlations Studies

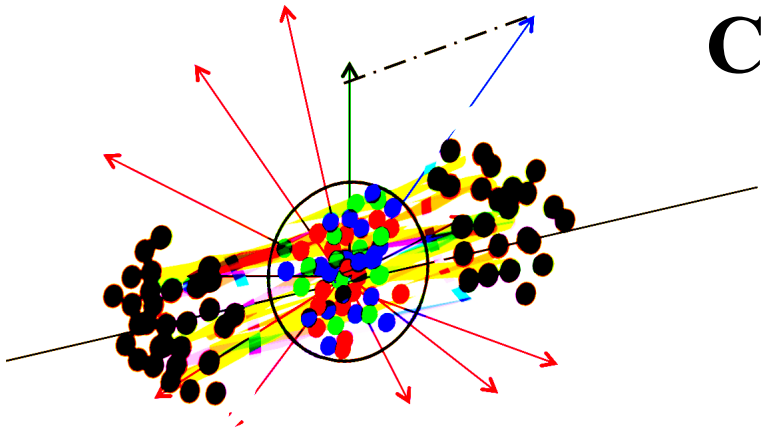

Event-by-event mean transverse momentum fluctuations

The fluctuations of thermodynamic quantities were proposed as a probe of the phase transition to the QGP formation.

Event by event <pT> fluctuations on the SPM

The variable F_{pT} measures the mean transverse momentum fluctuations as a function of the number of participants on collisions.

F_{pT} quantifies the observed fluctuations deviations of the statistically independent particle emission.

$$F_{p_T} = \frac{\omega_{data} - \omega_{random}}{\omega_{random}}$$

where ω is given by $\omega = \frac{\sqrt{\langle p_T^2 \rangle - \langle p_T \rangle^2}}{\langle p_T \rangle}$.

$$F_{p_T} = \frac{\phi}{\sqrt{\langle z^2 \rangle}} = \frac{1}{\sqrt{\langle z^2 \rangle}} \sqrt{\frac{\langle Z^2 \rangle}{\langle \mu \rangle}} - 1$$

For each particle we define a $z_i = p_{T_i} - \langle p_T \rangle$ and also a $Z_i = \sum_{j=1}^{N_i} z_j$, with N_i the numer of particles produced in an event i.

$$\langle z^2 \rangle = \frac{\sum_{i=1}^{N_{eventos}} \sum_j \left(\frac{n_j S_{nj}}{S_1}\right)^{1/2} \mu_1 \left[\left(\frac{n_j S_1}{S_{nj}}\right)^{1/4} \langle p_T \rangle_1 - \langle p_T \rangle\right]^2}{\sum_{i=1}^{N_{eventos}} \sum_j \left(\frac{njS_{nj}}{S_1}\right)^{1/2} \mu_1} \tag{3}$$

$$\frac{\langle Z^2 \rangle}{\langle \mu \rangle} = \frac{\sum_{i=1}^{N_{eventos}} \left[\sum_j \left(\frac{n_j S_j}{S_1}\right)^{1/2} \mu_1 \left[\left(\frac{n_j S_1}{S_{n_j}}\right)^{1/4} \langle p_T \rangle_1 - \langle p_T \rangle\right]\right]^2}{\left[\sum_{i=1}^{N_{eventos}} \sum_j \left(\frac{n_j S_{n_j}}{S_1}\right)^{1/2} \mu_1\right]} \tag{4}$$

By fitting the transverse momentum distributions data [4][5], we obtain the string density corresponding to the different multiplicities for pp collisions at $\sqrt{s} = 0.9, 2.76$ and 7 TeV. We aprpoximate $\langle \sum_j n_j \rangle$ and $\frac{S_{nj}}{S_1}$ from equations (3) and (4) as $\langle \sum_j n_j \rangle \sim N_s$ and $\frac{S_{nj}}{S_1} \sim \epsilon \left(\frac{R_p}{r_0}\right)^2$, with ϵ an effective centrality.

$$\epsilon = \left(\frac{R_p}{r_0}\right)^2 \frac{\zeta^t}{N_s^{max}} = \frac{\zeta^t}{\zeta^t_{max}} \tag{5}$$

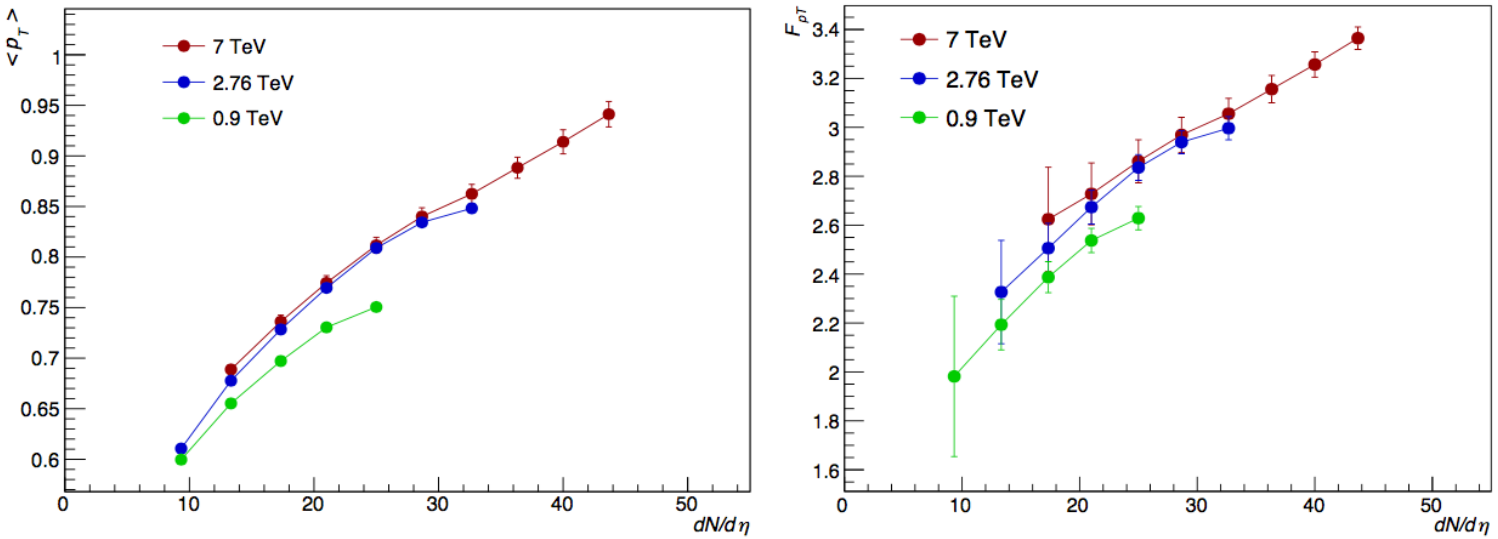

Figure 3: SPM $\langle p_T \rangle$ and F_{p_T} for pp collisions at .9,2.76 and 7 TeV.

4. S. Chatrchyan *et al.* [CMS Collaboration], Eur. Phys. J. C **72** (2012) 2164.
5. S. T. Heckel [ALICE Collaboration],Phys. Rept. **599** (2015) 1.

We consider F_{p_T} from equation (2) as a function of $\langle p_T \rangle$, N_s and ϵ function, depen-dending on ζ^t and $F(\zeta^t)$ in $\langle p_T \rangle$ and ϵ respectively.

$$\sqrt{\frac{\langle Z^2 \rangle}{\langle \mu_1 \rangle}} \simeq \left[N_s \langle p_T \rangle_1^2 \mu_1 - 2 N_s^{3/4} \epsilon^{1/4} \left(\frac{R_p}{r_0} \right)^{1/2} \langle p_T \rangle_1 \langle p_T \rangle + + N_s^{1/2} \epsilon^{1/2} \left(\frac{R_p}{r_0} \right) \mu_1 \langle p_T \rangle^2 \right]^{1/2} \tag{6}$$

$$\sqrt{\langle z^2 \rangle} \simeq \left[N_s^{1/2} \epsilon^{1/2} \left(\frac{r_0}{R_p} \right) \langle p_T \rangle_1^2 - 2 N_s^{1/4} \epsilon^{1/4} \left(\frac{r_0}{R_p} \right)^{\frac{1}{2}} \langle p_T \rangle_1 \langle p_T \rangle + \langle p_T \rangle^2 \right]^{1/2} \tag{7}$$

For comparing with the experimental measurements [5], we need to use the two particle correlator C_m for multiplicity class m and the $\langle p_T \rangle$ relative fluctuations $(\sqrt{C_m}/M(p_T)_m)$ for multiplicity class m.
We can relate $C = \langle \Delta p_{T,i}, \Delta p_{T,j} \rangle$ with F_{p_T} as:

$$\langle \Delta p_{Ti}, \Delta p_{Tj} \rangle \simeq 2 F_{p_T} \frac{var(p_T)}{\langle N \rangle} \tag{8}$$

With $\langle N \rangle$ being the mean multiplicity and $var(p_T)$ the variance of p_T.

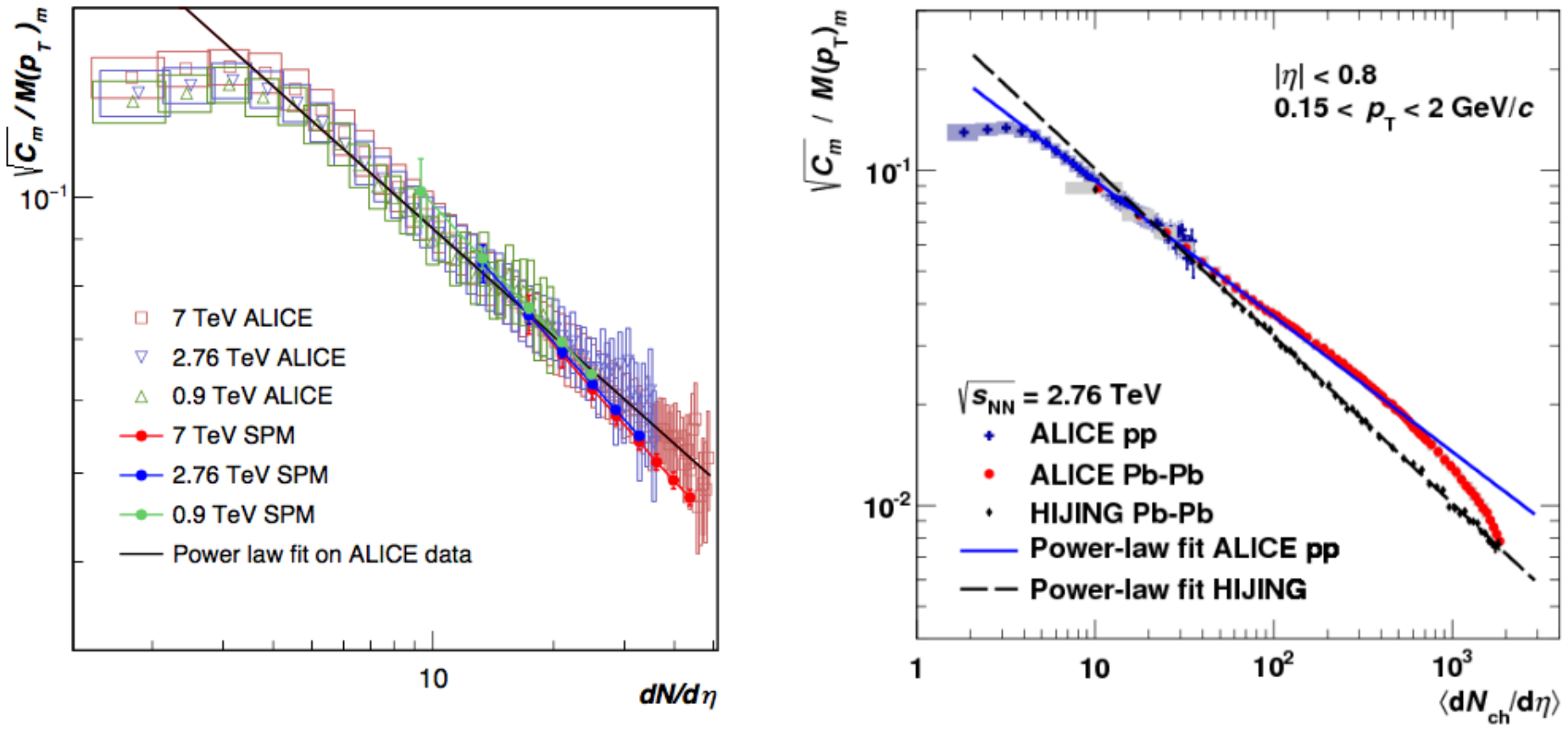

Figure 5: $\sqrt{C_m}/M(p_T)_m$ with the ALICE experimental data [5]

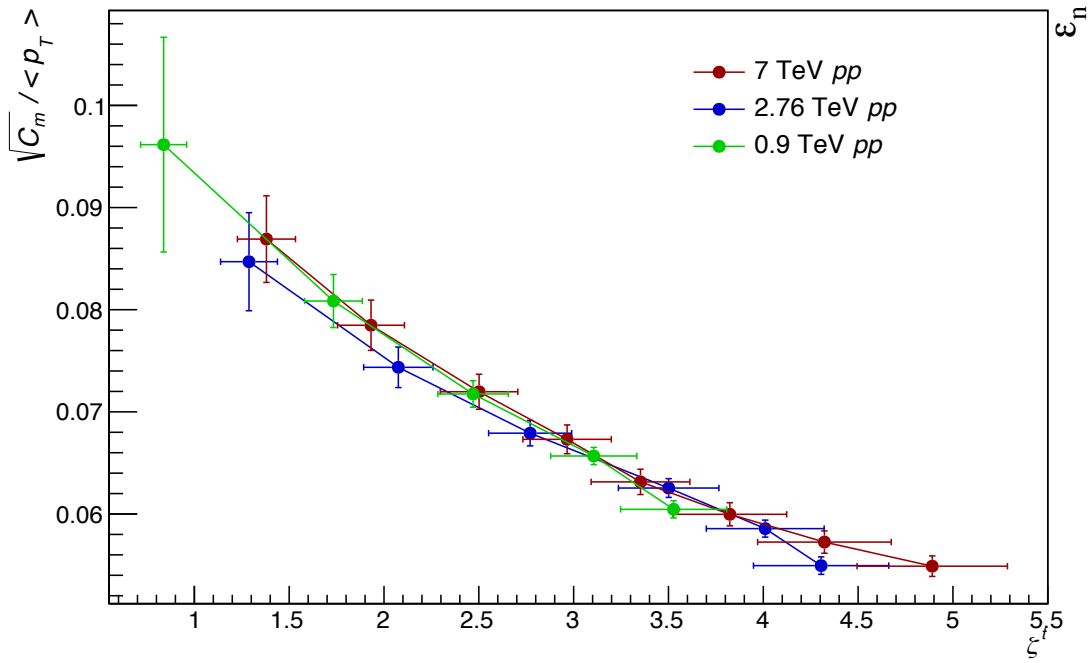
$\sqrt{C_m}/\langle p_T \rangle$
7 TeV *pp*
2.76 TeV *pp*
0.9 TeV *pp*
ξ_t

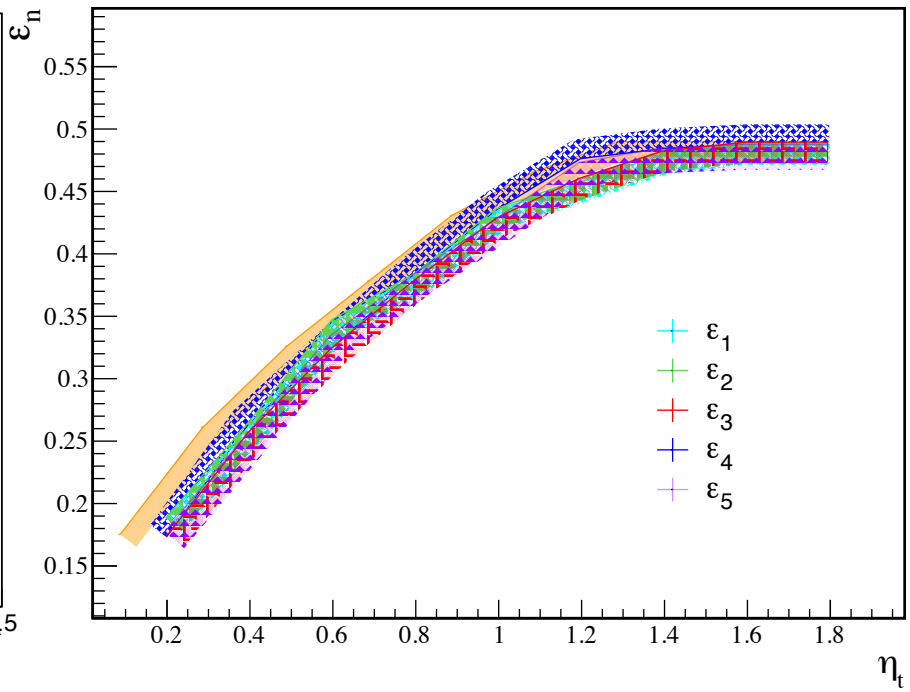
ε_n
ε_1
ε_2
ε_3
ε_4
ε_5
η_t

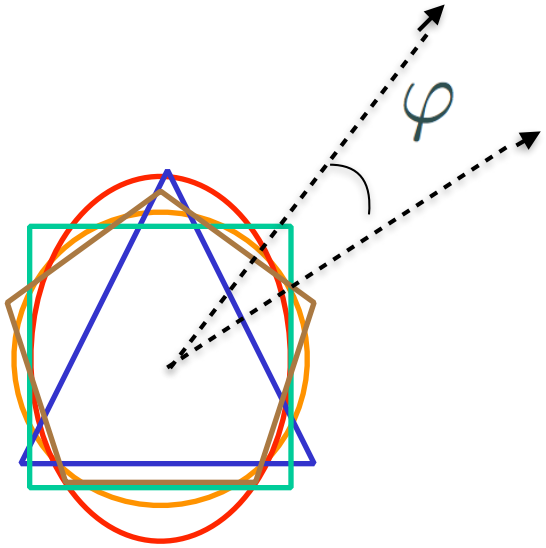
φ

viscosity of the droplet

Viscosity = Bulk viscosity + Shear viscosity

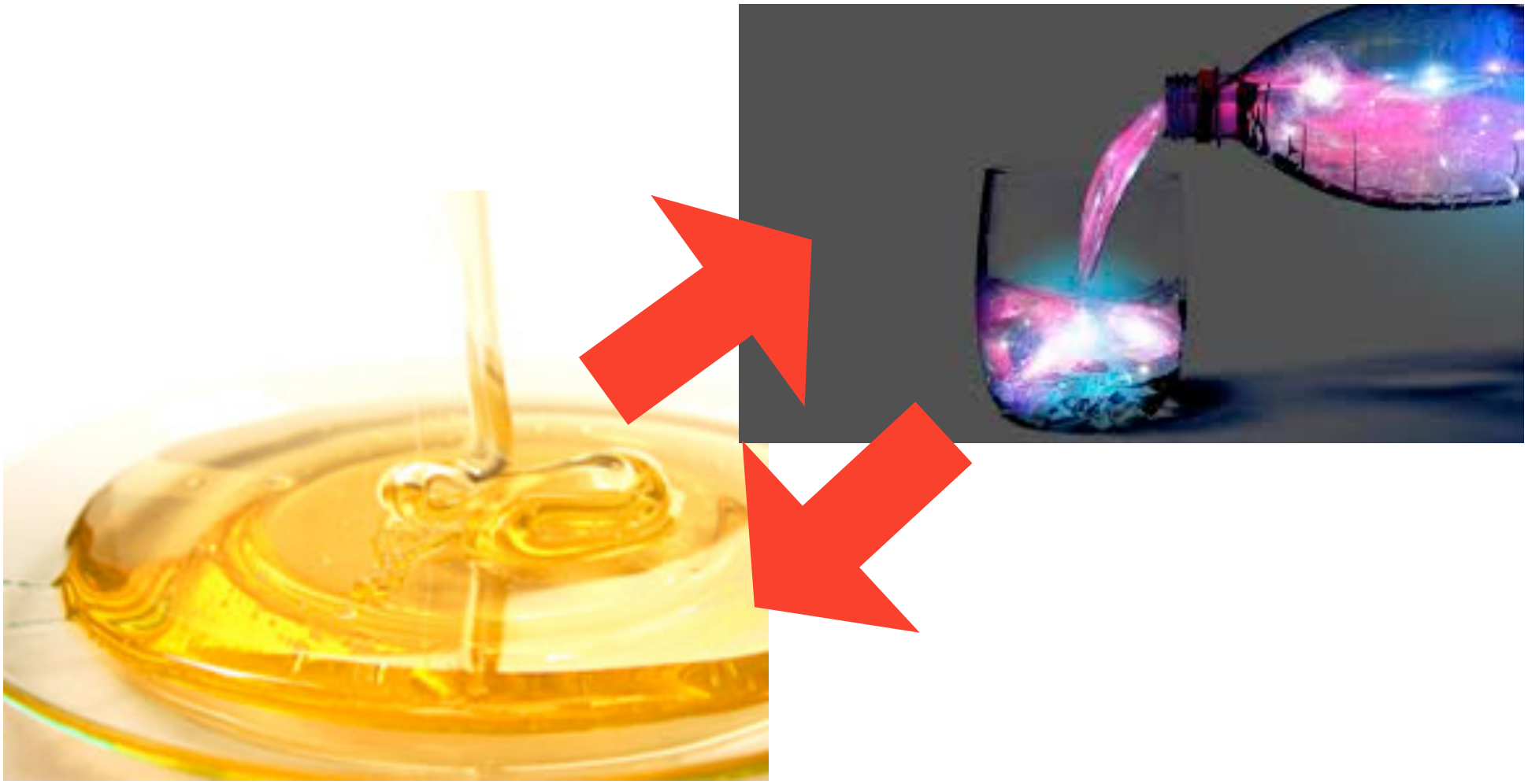

The fluid/shear viscosity is a measured of its resistance to gradual deformation by shear tensions, shear stresses or tensile stresses

Characteristic property of all fluids this emerge from the particle collision moving at different velocities generating resistance to it's moving

When fluid moves in a tube the particles move faster near the longitudinal axis of the tube and more slower near the walls. Therefore it generates a pressure difference to pass the friction resistance between layers to allow fluids.

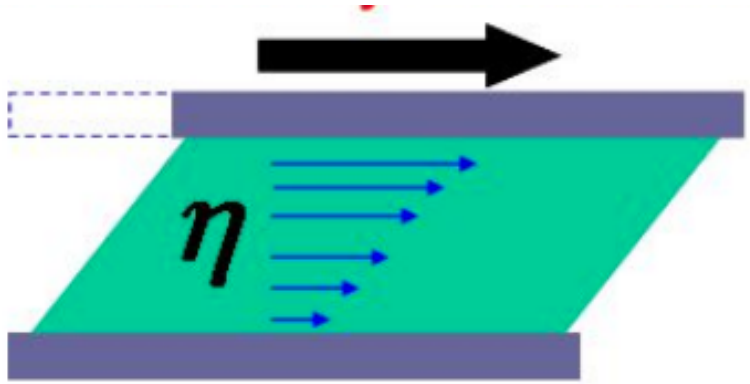

Bulk viscosity measures the degree of compressibility or dilatation

Volume viscosity is mainly related to the vibrational energy of the molecules

The volume viscosity is important in describing sound attenuation and the absorption of sound energy into the fluid depends on the sound frequency i.e. the rate of fluid compression and expansion. For an incompressible liquid the volume viscosity is superfluous

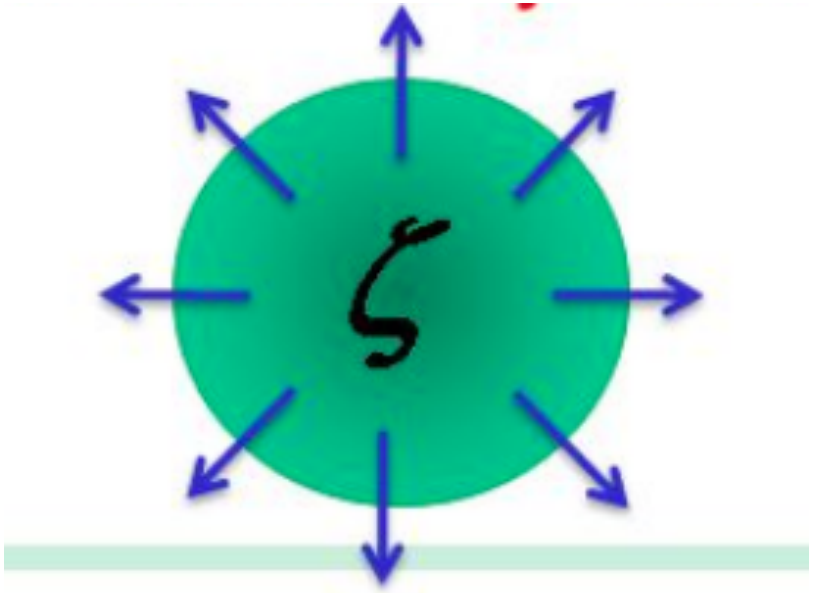

In the kinetic theory $\eta/s \simeq \frac{T\lambda_{fp}}{5}$

mean free path $\lambda_{mfp} \sim \frac{1}{n\sigma_{tr}}$

effective n density number of sources by volume unit

$$n = \frac{N_{sources}}{S_N L}$$

Considering $\frac{N_{sources}}{S_N L}\sigma_{tr} = (1 - e^{-\zeta^t})/L$

with L=1fm as the longitudinal extension of the source

$$\frac{\eta}{s} = \frac{TL}{5(1 - e^{-\zeta^t})}$$

Shear viscosity

Trace value of the energy momentum tensor of the matter which is a energy density

$$\langle \Theta^{\mu}_{\mu} \rangle = \varepsilon - 3P$$

Dias de Deus, Hirsch, Pajares, Scharenberg, Srivastava, Eur. Phys. J. C 72,2123 (2012)

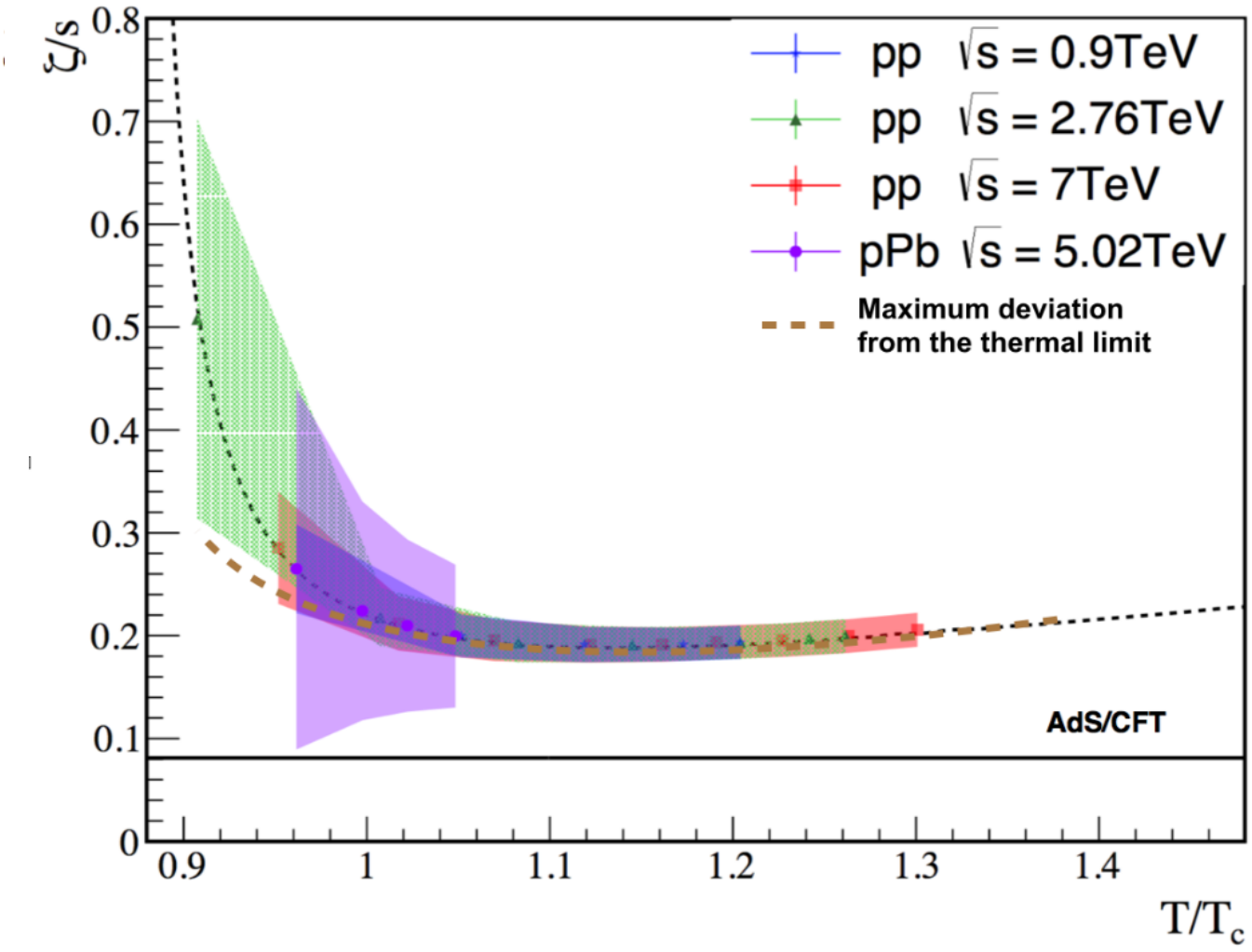
ζ/s
0.8
0.7
0.6
0.5
0.4
0.3
0.2
0.1
0
0.9
1
1.1
1.2
1.3
1.4
T/T_c
pp √s = 0.9TeV
pp √s = 2.76TeV
pp √s = 7TeV
pPb √s = 5.02TeV
Maximum deviation
from the thermal limit
AdS/CFT

$$\langle \Theta^{\mu}_{\mu} \rangle = \varepsilon - 3P$$

Trace anomaly $$\frac{\varepsilon - 3P}{T^4} = \left(\frac{\eta}{s}\right)^{-1} = \Delta$$

The Pressure can be obtained from shear viscosity over entropy relation and the Bjorken energy is related to the multiplicity considering the area S and the relaxation time

$$\varepsilon = \frac{3N_{part}\langle E \rangle}{2\tau S}\frac{dN}{dy} \qquad P = \frac{1}{3}\left(\varepsilon - \frac{T^4}{\eta/s}\right) \quad s = (\varepsilon + P)/T$$

Sound velocity

$$c_s^2 = \left(\frac{\zeta^t e^{-\zeta^t}}{1 - e^{-\zeta^t}} - 1 \right) \left[\frac{0.019\Delta}{3(1 - e^{-\zeta^t})} - 0.33 \right]$$

$$c_s^2 = \left(\frac{e^{-\zeta^t}}{F^2} - 1 \right) \left[\frac{0.019\Delta}{3\zeta^t F^2} - 0.33 \right]$$

momentum operator proyector method

Bulk viscosity

$$\frac{\zeta}{\tau_\Pi} = \left(\frac{1}{3} - c_s^2 \right) (\varepsilon + P) - \frac{2}{9}(\varepsilon - 3P)$$

relaxation time

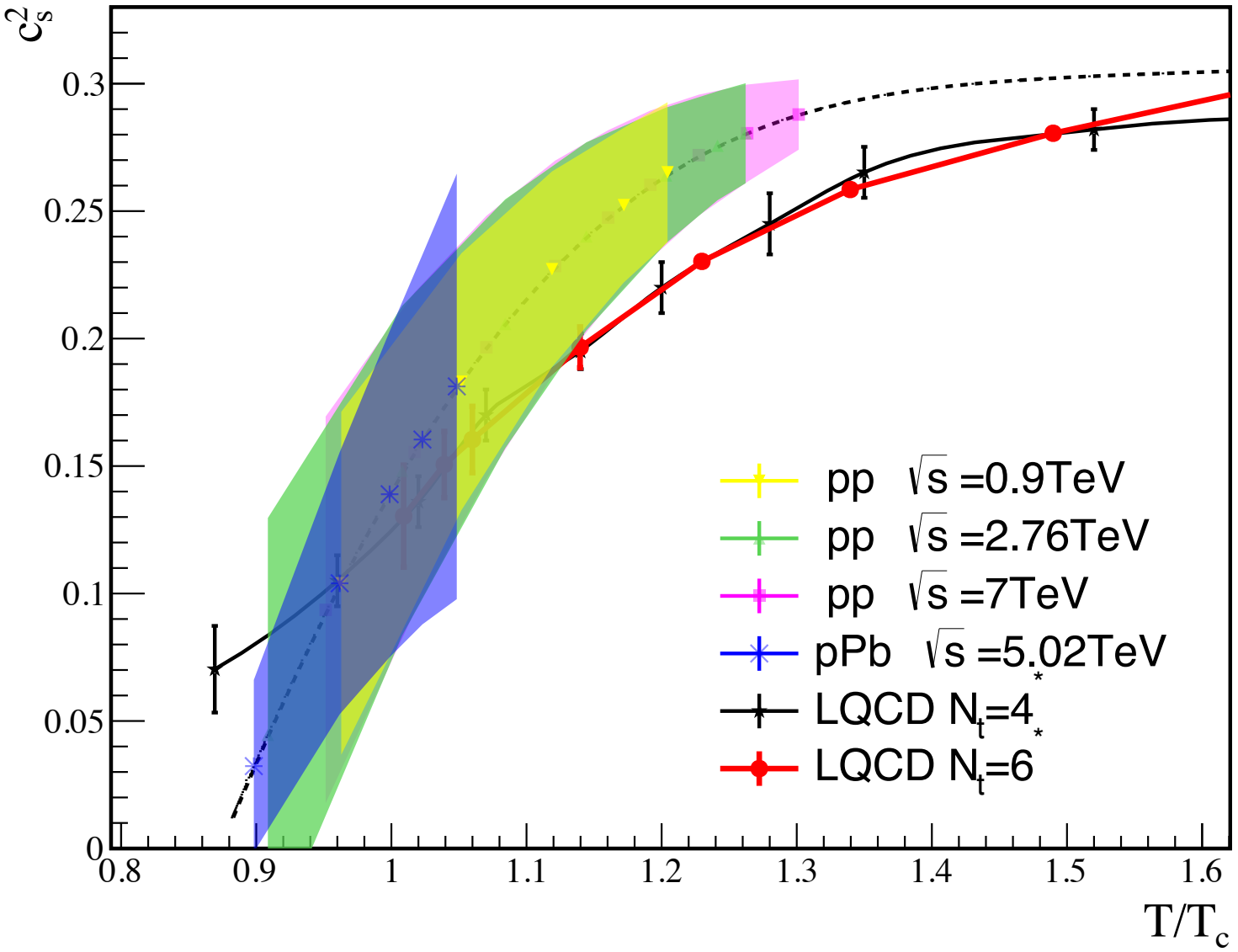
c_s^2
0.3
0.25
0.2
0.15
0.1
0.05
0
0.8
0.9
1
1.1
1.2
1.3
1.4
1.5
1.6
T/T_c
pp $\sqrt{s}$ =0.9TeV
pp $\sqrt{s}$ =2.76TeV
pp $\sqrt{s}$ =7TeV
pPb $\sqrt{s}$ =5.02TeV
LQCD N_t=4*
LQCD N_t=6

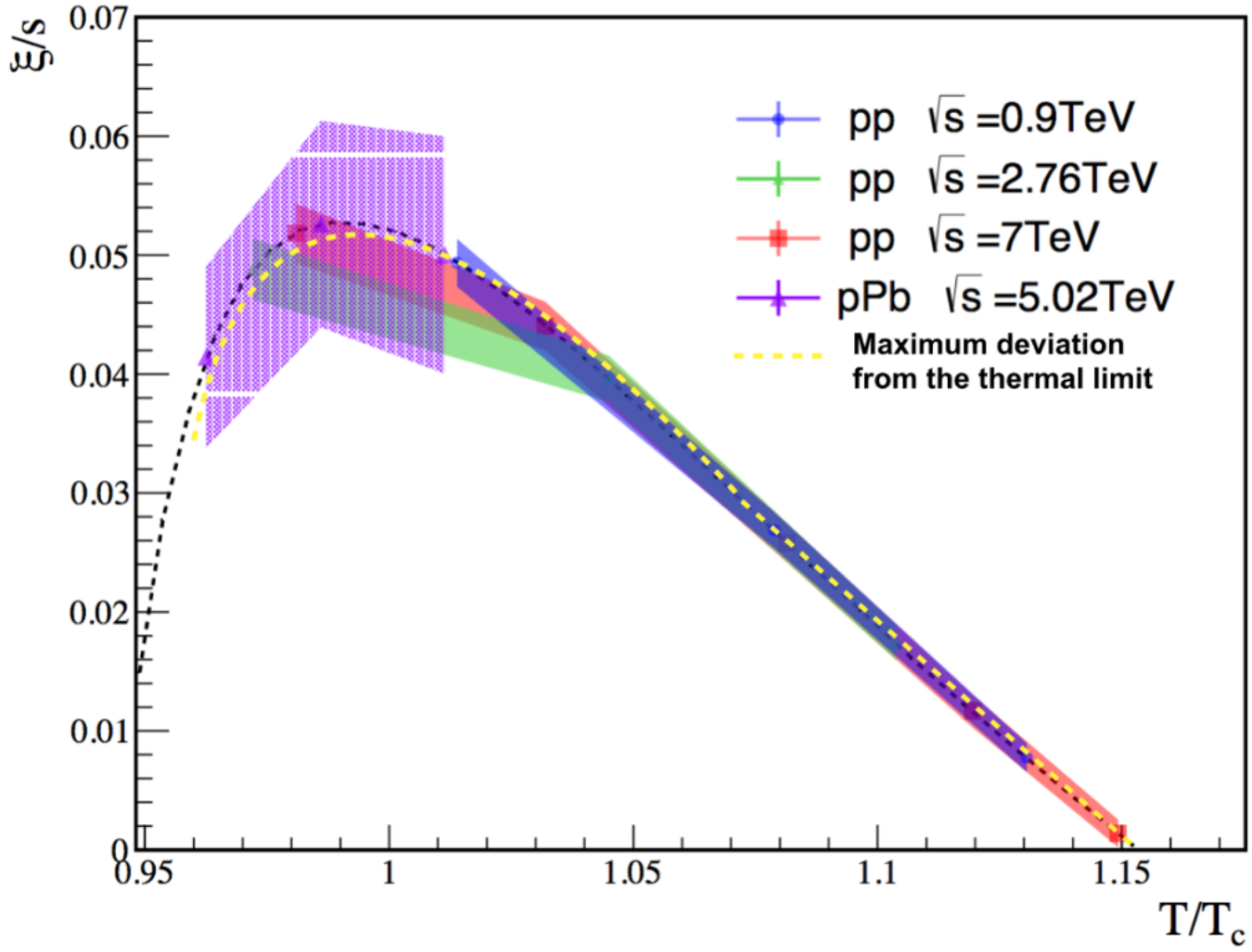
ξ/s
0.07
0.06
0.05
0.04
0.03
0.02
0.01
0
0.95
1
1.05
1.1
1.15
T/T_c
pp √s =0.9TeV
pp √s =2.76TeV
pp √s =7TeV
pPb √s =5.02TeV
Maximum deviation
from the thermal limit

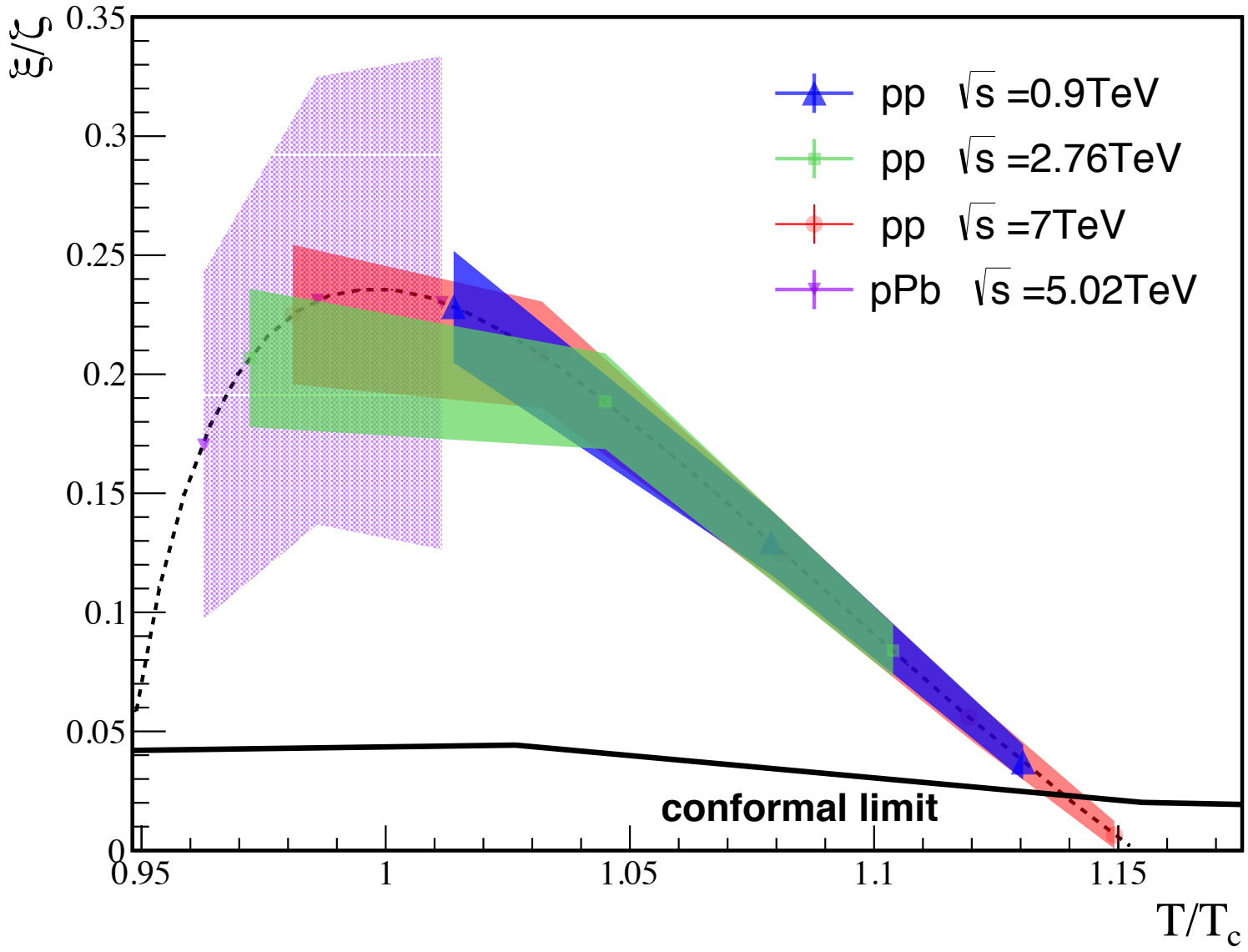

Phys.Lett.B663:286-289,2008

Conclusions

- The results on EbE mean transverse momentum fluctuations are consistent with data and the small change of slope may also give indication of a phase transition
- Contribution to flow modes emerge from initial state geometry are driving by the same universal trend given by the color reduction function
- There is an important contribution from the initial geometry for the phase transition threshold and that drives important differences among the collectivity and phase transition contrary to AA collisions.
- Consequences and implications are straightforward seen in the initial anisotropy, flow and transverse momentum fluctuations.
- The contribution and limits on geometry effects on the shear and bulk viscosity are presented, indicating that the initial geometry gives significant differences on the velocities of the emitted particles that generates resistance to the flow but not on the contribution of the degree of compressibility which is intrinsic of the medium

- String percolation threshold for elliptically bounded systems, J.E. Ramirez, I. Bautista, A. Fernández. Physica 488 (2017) 8-15.
- Heavy-ion physics at the LHC: Review of Run I results, Renu Bala (Jammu U.), Irais Bautista (Puebla U., Mexico), Jana Bielcikova (Rez, Nucl. Phys. Inst.), Antonio Ortiz (Mexico U., ICN), Int.J.Mod.Phys. E, Vol.25, Pag.1-28
- Indication of change of phase in high-multiplicity proton-proton events at LHC in String Percolation Model, I. Bautista, A. Fernandez Téllez (Puebla U., Mexico), Premomoy Ghosh (Calcutta, VECC), Phys.Rev. D, Vol.92, Pag.0-0.
- ICHEP Proceedings, Chicago 2016
- QCD Challenges from pp to AA, Puebla 2017
- Presentation on ISMD, Tlaxcala 2017
- QM18 Poster contribution

köszönöm !!!

SPONSORS

THE 7TH CONFERENCE ON LARGE HADRON COLLIDER PHYSICS

May 20th - 25th, 2019

PUEBLA - BUAP

Registration: www.lhcp2019.buap.mx

LOCAL ORGANIZING COMMITTEE

A. Ayala (UNAM)
I. Bautista (BUAP)
S. Carrillo (IBERO)
H. Castilla (CINVESTAV)
E. Cuautle Flores (UNAM)
E. de la Cruz Burelo (CINVESTAV)
L. Díaz Cruz (BUAP)
A. Fernández Téllez (BUAP)
Ivan Heredia (CINVESTAV)
A. Ortíz Velázquez (UNAM)
G. Paic (UNAM)
I. Pedraza Morales (BUAP)
Pablo Roig (CINVESTAV)
M. Rodríguez Cahuantzi (BUAP)
Ma. Elena Tejeda Yeomanns (UNISON)

TECHNICAL SECRETARIAT

Dawn Hudson (CERN)
Connie Potter (CERN)

SCIENTIFIC SECRETARIES

M. Martínez Gutiérrez (BUAP)
Pablo Roig (CINVESTAV)

CONFERENCE CHAIRS

A. Nisati (INFN)
J. Olsen (PRINCETON UNIV.)
A. Fernández Téllez (BUAP)
I. Bautista (BUAP)
B. Mansoulie
INTERNATIONAL CO-CHAIR
G. Mitselmakher - IAC DEPUTY CHAIR